10-19-2015

FLOW-INDUCED VIBRATION OF A FLEXIBLE CIRCULAR CYLINDER

Haoyang Cen
University of Windsor

Flow-Induced Vibration of a Flexible Circular Cylinder

By

Haoyang Cen

A Thesis
Submitted to the Faculty of Graduate Studies
through the Department of Mechanical, Automotive & Materials Engineering
in Partial Fulfillment of the Requirements for
the Degree of Master of Applied Science
at the University of Windsor

Windsor, Ontario, Canada

2015

Flow-Induced Vibration of a Flexible Circular Cylinder

by

Haoyang Cen

APPROVED BY:

_____

R. Seth
Department of Civil and Environmental Engineering

_____

V. Stoilov
Department of Mechanical, Automotive & Materials Engineering

_____

R. Carriveau, Co-Advisor
Department Civil and Environmental Engineering

_____

D. Ting, Advisor
Department of Mechanical, Automotive & Materials Engineering

October 14, 2015

DECLARATION OF CO-AUTHORSHIP/PREVIOUS PUBLICATIONS

I hereby declare that this thesis incorporates material that is the result of joint research, as follows:

Thesis Chapter	**Details**
Chapter 2	This thesis also incorporates the outcome of a joint research undertaken in collaboration with Mojtaba Ahmadi-Baloutaki under the supervision of Dr. Rupp Carriveau and Dr. David S-K. Ting. In all cases, the key ideas, primary contributions, data analysis and interpretation, were performed by the author, and the contribution of the co-author was primarily through the provision of wording and formatting.

I am aware of the University of Windsor Senate Policy on Authorship and I certify that I have properly acknowledged the contribution of other researchers to my thesis, and have obtained written permission from each of the co-author(s) to include the above material(s) in my thesis.

I certify that, with the above qualification, this thesis, and the research to which it refers, is the product of my own work.

I hereby declare that this thesis includes two original papers that have been previously published/submitted for publication in peer reviewed journals, as follows:

Thesis Chapter	**Publication title**	**Publication status**
Chapter 2	H. Cen, M. Ahmadi-Baloutaki, D. S.-K. Ting, and R. Carriveau, "Mitigating Flow-Induced Vibration of a Flexible Circular Cylinder via Pre-tension," Sustainable Energy Technologies and Assessments, In Press.	Published
Chapter 3	H. Cen, R. Carriveau and D. S-K. Ting, "Effect of Mass Ratio on the Hydrodynamic Response of a Flexible Cylinder", Journal of Marine Science and Application	Under review

I certify that I have obtained a written permission from the copyright owner(s) to include the above submitted material(s) in my thesis. I certify that the above material describes work completed during my registration as a graduate student at the University of Windsor.

I certify that, to the best of my knowledge, my thesis does not infringe upon anyone's copyright nor violate any proprietary rights and that any ideas, techniques, quotations, or any other material from the work of other people included in my thesis, published or otherwise, are fully acknowledged in accordance with the standard referencing practices. Furthermore, to the extent that I have included copyrighted material that surpasses the bounds of fair dealing within the meaning of the Canada Copyright Act, I certify that I have obtained a written permission from the copyright owner(s) to include such material(s) in my thesis and have included copies of such copyright clearances to my appendix.

I declare that this is a true copy of my thesis, including any final revisions, as approved by my thesis committee and the Graduate Studies office, and that this thesis has not been submitted for a higher degree to any other University or Institution.

ABSTRACT

The offshore industry is currently experiencing challenges in designing flexible risers, cables etc., due to their susceptibility to FIV. Deeper understanding of the physics behind FIV is necessary in developing risers etc. This work presents two sets of experimental studies, collectively focusing on critical parameters that may greatly influence cylinder's hydrodynamic response. A Tygon tube was towed from rest to steady speed before slowing down to rest again in still water. Axial pre-tension and mass ratio was varied for parametrically studying their effects on the cylinder's hydrodynamic response, which was characterized mainly by vibration amplitudes and frequencies. The resulting effects of varying profile on flow-vibration amplitudes and frequencies have been quantified and expressed with respect to reduced velocity. A 2D numerical study has also been conducted to study the wake behind a circular cylinder, showing 4 types of vortex shedding modes.

DEDICATION

To my family.

ACKNOWLEDGEMENTS

This thesis would not have been completed without the guidance of my advisors, Dr. David S-K Ting and Dr. Rupp Carriveau in the past few years. I would like to extend my sincere thanks to them for their constant guidance and patience that have helped me grow. I have truly enjoyed working with them in the Turbulence & Energy Laboratory. I would also like to thank the remaining members of my committee, Dr. Rajesh Seth and Dr. Vesselin Stoilov for offering their comments to keep me on track in my research. Great thanks must also be given to the members of the Turbulence & Energy Laboratory, in particular Jamie C. Smith, for their guidance in my research and study. Acknowledgement should also be made to the laboratory technologists, particularly Andy Jenner and Matthew St. Louis, for the technical assistance they have provided.

This work has been supported by the Natural Sciences and Engineering Research Council of Canada.

TABLE OF CONTENTS

LIST OF TABLES

CHAPTER II: MITIGATING FLOW-INDUCED VIBRATION OF A FLEXIBLE CIRCULAR CYLINDER VIA PRE-TENSION

CHAPTER III: EFFECT OF MASS RATIO ON THE HYDRODYNAMIC RESPONSE OF A FLEXIBLE CYLINDER

LIST OF FIGURES

CHAPTER I: INTRODUCTION

CHAPTER II: MITIGATING FLOW-INDUCED VIBRATION OF A FLEXIBLE CIRCULAR CYLINDER VIA PRE-TENSION

CHAPTER III: EFFECT OF MASS RATIO ON THE HYDRODYNAMIC RESPONSE OF A FLEXIBLE CYLINDER

APPENDIX A: DETERMINATION OF TOWING SPEED

CHAPTER I

INTRODUCTION

1 Background

Flow-induced vibration (FIV) is a multi-disciplinary subject involving fluid and structural mechanics and vibrations [1]. It occurs and affects heavily many engineering applications where structures are subject to flowing fluid, such as power transmission lines, bridge decks and skyscrapers etc. Both destructive and useful motions on structures could be potentially caused by the interactions between the structure and moving fluid. In particular, offshore industry is one of the most vulnerable fields to FIV due to the extensive constructions in flowing water. Drilling risers, catenaries, marine cables and underwater pipelines are a few examples that are highly susceptible to FIV. In the absence of proper mitigation, FIV could potentially lead to: clashing of adjacent risers when multiple risers are present; increased dynamic load that could result in fatigue damage or even premature failure. Thus, it is considered to be a major concern throughout the development of offshore structures, which includes conceptualization, design, assessment, construction and maintenance. In the presence of FIV, the total project cost was estimated by British Petroleum to increase by approximately 10 %.

In the past decades the offshore explorations have advanced to deeper water, extending from around 100 m in 1965 to over 3000 m in 2009 [2]. This, in concurrence with materials being pushed to their limits, has led to progressively lighter, more flexible, and more slender offshore structures. Due to these geometrical characteristics, the

aforementioned slender offshore structures are prone to FIV with highly-coupled torsional, axial and lateral flexibility [3]. Therefore, it is critical to include particularly careful consideration in their design stages to achieve prediction, reduction, suppression and mitigation of FIV without the tradeoff of increasing drag force. This requires enhanced understanding of the underlying interaction mechanism in FIV. Among many others, experimentation and numerical simulation are two viable approaches to gain more insights into this problem.

Ideally, field experiment using real models in their real service locations is the best way to examine the occurrence and level of FIV. However, it is a costly process and the uncertainties in current make the conduction of experiment under desired conditions extremely difficult and challenging. Alternatively, laboratory testing is an appealing way for parametric investigation to produce high quality data by manipulating input parameters. The limitation of laboratory testing is that realistic fluid condition (high Reynolds numbers, turbulent flows, shear flows etc.) as well as model characteristics (high aspect ratios, mass ratios etc.) are challenging to achieved due to constrains in the scale of testing facility and complicated instrumentation.

Numerically, computational fluid dynamics (CFD) occurs to be a promising way of investigating FIV since it is theoretically able to depict every detail in the interaction between structures and fluids. However, it is not yet considered a mature approach, especially in 3-dimensional scenarios due to the overwhelming computational time. More efficient computation technique and computer resources are in great need to develop this approach.

2 The phenomenon of FIV

When a bluff body, like the aforementioned structures, is immersed in a flowing fluid, excitations from the fluid would cause it to vibrate and therefore interactively change the flow condition. This is so-called flow-induced vibration. Though these excitations are known to come from flowing fluid, the inducing sources still would vary. Many ways of classifying flow-induced vibrations have been proposed. Weaver [4] classified the sources of excitation based directly on the nature of the vibration: (i) forced vibrations induced by turbulence; (ii) self-controlled vibrations, in which some periodicity exists in the flow, independent of motion; (iii) self-excited vibrations. Other than that, a phenomenological classification was proposed by Blevins [1]. He classified vibrations sources into: (i) steady flow and (ii) unsteady flow. The former one are then subdivided into 'instabilities' (i.e. self-excited vibrations) and vortex-induced vibrations, while the latter subdivided into: random, e.g. turbulence-related; sinusoidal, e.g. wave-related; and transient oscillations, e.g. water-hammer problems.

Naudascher & Rockwell [5, 6] proposed a classification systematically and logically in terms of the sources of excitation of flow-induced vibration, namely, (i) extraneously induced excitation; (ii) instability-induced excitation; and (iii) movement-induced excitation. This classification will be used more extensively in our study. Extraneously induced excitation is defined as due to fluctuations in the flow or pressure, independent of any flow instability and any structural motion, e.g. turbulence buffeting. Instability induced excitation is associated with a flow instability and involves local flow oscillations, e.g. alternate vortex shedding from a cylindrical structure. Finally,

movement induced excitation is the result from movements of the body, e.g. flutter of an aircraft. This classification will be used more extensively in our study.

3 Important parameters for analysis

A great deal of research effort has been directed to flow-induced vibration on circular cylinder, starting from stationary ones, to elastically mounted, and flexible. Different parameters ranging from describing flow characteristics to geometrical ones have been used in this investigation. These intensively used parameters are summarized into three groups in a fashion similar to [7]. Those in the first and second categories are related to flow conditions and model's structural aspects respectively, while the third one is describing the interaction between the structure and fluid.

3.1 Flow parameters

Parameters described in this section are related to fluid flow properties.

Reynolds number (Re) characterizes dynamically similar flows, i.e., flows that have geometrical similarities in terms of streamlines and submerged objects. It is defined as:

$$\mathrm{Re} = \rho_f \frac{U \cdot D}{\mu} = \frac{U \cdot D}{\nu} \tag{1.1}$$

where, ρ_f is fluid density; U is free stream velocity; D is a characteristic dimension of the submerged object, which in the present study is the cylinder's outer diameter; μ and υ are the dynamic and kinematic viscosity of fluid respectively.

Turbulence intensity is a relative measure of the amount of fluctuations in the flow. Usually it is expressed as:

$$\frac{u_{rms}}{U_{mean}} \tag{1.2}$$

with u_{rms} the root mean square of the velocity fluctuation; U_{mean} the mean free stream velocity.

3.2 Structural parameters

These parameters describe the properties of the model under investigation and they are related to structure aspects.

Damping ratio (ζ_s) is representation of the structure's ability to dissipate energy in a cycle of motion. It is the ratio of the linear damping coefficient to its critical value, as expressed in the below equation:

$$\zeta_s = \frac{c}{2\sqrt{m_s k}} = \frac{c}{2m_s \omega_n} \tag{1.3}$$

where, c is the damping coefficient; ω_n is the natural frequency. It should be noted that for a given vibration mode of a flexible cylinder, there is a corresponding damping coefficient and natural frequency. The value of damping ratio for a given mode can be obtained experimentally by carrying out decay test.

Mass ratio (m^*) describes the relative weights between the test model and fluid. It is defined as the ratio of the structural mass over the mass of displaced fluid, as expressed below:

$$m^* = \frac{m_s}{m_f} \tag{1.4}$$

with m_s the structural mass of the test model; m_f the mass of corresponding displaced fluid. In issues of vibration, it is common to expect added mass to the system due to its acceleration and deceleration. Therefore, the mass ratio is typically expressed with or without the inclusion of added mass in literature. However, the added mass is not included in the consideration of mass ratio throughout the present study.

Aspect ratio (*AR*) a parameter reflecting the geometric characteristic of a structure, which for a circular cylinder is defined as its length over the diameter

$$AR = \frac{L}{D} \tag{1.5}$$

where, L is the cylinder's length and D is the cylinder's diameter.

Roughness ratio (R_a) is a relative measure of the model's surface roughness. It is normally non-dimensionalized by the model's diameter for a circular cylinder, as

$$R_a = \frac{k}{D} \tag{1.6}$$

where, k is a characteristic dimension of the roughness on the model's surface. Roughness ratio is one of the parameters that greatly influence the flow condition by varying the contact surface's friction and therefore the boundary layer. Among others, more intensive turbulence and varied vortex shedding pattern are two immediate results.

3.3 Interaction parameters

There are some parameters that are related to both the test structure and fluid flow, as the problem under study is intrinsically fluid-structure interaction.

Non-dimensional amplitudes (A_x/D & A_y/D) are vibration amplitudes normalized by the cylinder's diameter. They are relative but straightforward means to describe the intensity of the undergoing vibration. The in-line non-dimensional amplitude, for example, is defined as

$$\frac{A_x}{D} \tag{1.7}$$

This also applies to the cross-flow direction.

Reduced velocity (U_r) is an important parameter in FIV. It is the ratio of travel distant per cycle over the cylinder's diameter, as defined as

$$U_r = \frac{U}{f_n \cdot D} \tag{1.8}$$

where, f_n is the natural frequency of the cylinder. Moe & Wu [8] proposed reduced velocity with the natural frequency in air which is called nominal reduced velocity and also with true vibration frequency which is called true reduced velocity. In the present work the fundamental natural frequency, which is the natural frequency of the test cylinder vibrating at its first mode, of the system in water (f_n) is used for the calculation of reduced velocity.

Strouhal number (St) is a dimensionless parameter describing oscillating flow mechanisms and is defined as

$$St = \frac{f_v \cdot D}{U} \tag{1.9}$$

where, f_v is the vortex shedding frequency. Investigations from different researchers have demonstrated that the Strouhal number in the wake of a cylinder is mainly dependent on the Reynold's number, as depicted in Fig. 1 [9], with a value of 0.2 over a wide region.

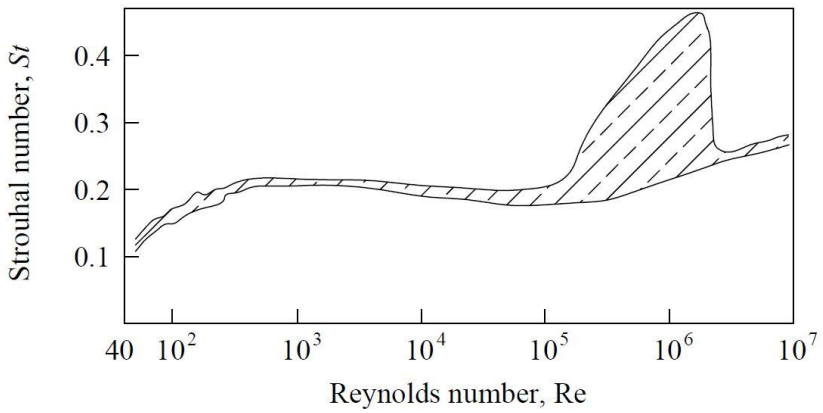

Fig. 1. Strouhal-Reynolds Number relationship for circular cylinders [9].

4 Mathematical theory

For cylindrical structures with high aspect ratios, for example drilling risers, they can be feasibly idealized as a beam with low flexural stiffness under the following assumptions [10]:

i. Planar surfaces orthogonal to the axis of the beam remain planar and orthogonal to the axis after the deformation. Therefore transverse shear is neglected;

ii. All the forces acting on the beam can be expressed by vectors in *x* or *y* axis;

iii. The transverse section of the beam is symmetric with respect to plane *xz* or *yz*.

In the case of slender flexible cylinders undergoing FIV, their responses are considerably more complex than that of short rigid cylinders. However, under the above set of assumptions, the planes perpendicular to the axis can be considered to remain as planes and being perpendicular to the axis under deformation. With that, the governing equation of a flexible cylinder, as depicted in Fig. 2, can be reasonably derived from that of a flexibly mounted rigid cylinder, using strip theory, where segments of the flexible cylinder are considered as a rigid cylinder [11, 12].

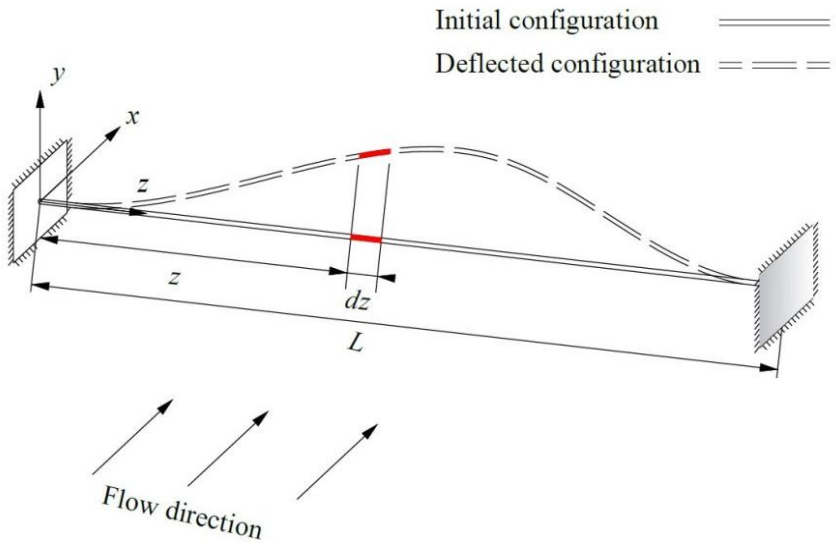

Fig.2. A flexible cylinder and its deformed shape under flowing fluid.

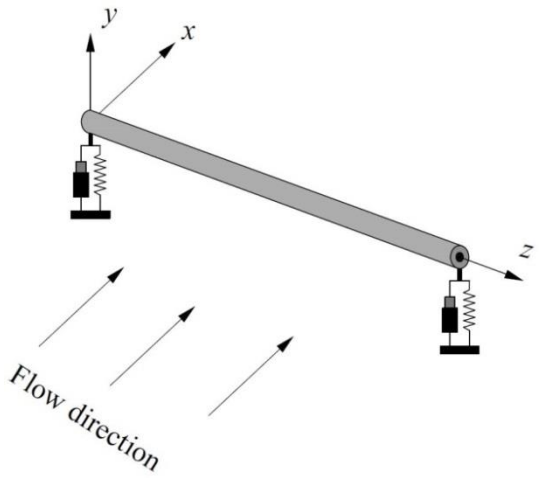

Fig.3. An elastically mounted rigid cylinder under uniform flow.

Considering a Cartesian axis reference system as depicted in Fig. 3, the ordinary differential equation governing the motion of a rigid cylinder of mass *m*, with one degree of freedom (depicted in Fig. 3), mounted on springs with spring constant *k* and dashpots with damping constant *b*, under a uniform current of velocity *U* can be expressed as:

$$m\frac{d^2y}{dt^2}+b\frac{dy}{dt}+ky=f(t) \tag{1.10}$$

with $f(t)$ representing the time-dependent external force acting on the rigid cylinder. One can see from this equation that the system's mass, spring constant, and damping constant are of great significance in its dynamic response upon external forces.

As depicted in Fig. 2, a Cartesian axis reference system similar to the one used in elastically mounted rigid cylinder is set up, with $u(z, t)$ and $v(z, t)$ denoting displacements in the x (in-line) and y (cross-flow) direction respectively. By applying strip theory, the equation governing a flexible cylinder of length L, mass per unit length m, structural damping b, bending stiffness EI and axial tension T, under an external force of $f(z, t)$ in the x direction, is given by:

$$m(z)\frac{\partial^2 u(z,t)}{\partial t^2} + b\frac{\partial u(z,t)}{\partial t} + EI\frac{\partial^4 u(z,t)}{\partial z^4} - \frac{\partial}{\partial z}\left(T(z)\frac{\partial u(z,t)}{\partial z}\right) = f(z,t) \tag{1.11}$$

Thus, for a given external force, the flexible cylinder's dynamic response is highly dependent on its structural properties (mass, damping, and bending stiffness) and the applied axial tension. This equation also applies to the y direction, for the cross-flow displacement $v(z, t)$. Upon the knowledge of the external force, its dynamic can be obtained by applying the appropriate boundary conditions. For a fixed-ends cylinder as the one in the present study, the corresponding boundary conditions are:

$$u(0,t) = 0, \qquad u(L,t) = 0$$
$$\frac{\partial u(0,t)}{\partial z} = 0, \quad \frac{\partial u(L,t)}{\partial z} = 0$$

5 Research objectives and scope

The overall research objective of the present work is to enhance the fundamental understanding of the physics and interaction mechanism behind flow-induced vibration

on a flexible circular cylinder. This understanding is critical in the development of offshore cables, pipelines etc. Ultimately it will lead to a more cost-effective and reliable offshore structures designs.

As revealed from the cylinder's governing equation, the cylinder's mass, damping, bending stiffness, and axial tension appear to be of dominance in its dynamic response. Thus, the scope of this work includes experimental investigations on the effect of axial pre-tension and mass ratio on the hydrodynamic response of a flexible circular cylinder, and a 2-dimensional numerical simulation on circular cylinder to study the wake downstream. This thesis is subdivided into 5 chapters to present the research and findings in a logical way. The second chapter describes an experimental study on the effect of axial pre-tension on the FIV of a flexible cylinder. Following, Chapter III contains a experimental work with a similar setup as that in Chapter II, but the focus of this chapter is to investigate the mass ratio on the dynamic response of a flexible cylinder. Due to the constraint in the experimental facility, the wake behind a circular cylinder with different mass ratio is investigated numerically, as presented in Chapter IV. In the last chapter of the present work, a summary of conclusions are addressed along with suggested future work.

References

[1] Blevins, R.D. (2001). Flow induced vibrations. Second Edition, Krieger Publishing Company, Malabar, Florida.

[2] Nixon, L.D., Shepard, N.K., Bohannon, C.M., Montgomery, T.M., Kazanis, E.G., Gravois, M.P., Kazanis, E.G., Conner, G.M., & Gravois, M.P. (2009). Deepwater

Gulf of Mexico 2009: Interim report of 2008 highlights. Technical report, US Department of Interior, Mineral Management Service.

[3] Sanaati, B., & Kato, N. (2012). A study on the effects of axial stiffness and pre-tension on VIV dynamics of a flexible cylinder in uniform cross-flow. *Applied Ocean Research*, **37**, 198–210.

[4] Weaver, D.S. (1976). On flow induced vibrations in hydraulic structures and their alleviation. *Canadian Journal of Civil Engineering*, **3**, 126–137.

[5] Naudascher, E., & Rockwell, D. (1980). Oscillator-model approach to the identification and assessment of flow-induced vibrations in a system. *Journal of Hydraulic Research*, **18**, 59–82.

[6] Naudascher, E., & Rockwell, D. (2012). Flow-induced vibrations: an engineering guide. Courier Corporation.

[7] Koushan, K. (2009). Vortex induced vibrations of free span pipelines. Ph.D. Thesis, Norwegian University of Science and Technology, Trondheim, Norway.

[8] Moe, G., & Wu, Z.J. (1990). The lift force on a cylinder vibrating in a current. *Journal of Offshore Mechanics and Arctic Engineering*, **112**(4), 297-303.

[9] Lienhard, I.H. (1966). Synopsis of lift, drag and vortex frequency data for rigid circular cylinders. Washington State University, College of Engineering, Research Division Bulletin 300.

[10] Masdemont-Soler, J. (2002). Curs d'elements finits amb aplicacions. First Edition. Pilitext Edicions UPC, Technical University of Catalonia.

[11] Triantafyllou, M.S. (2006). VIVA: Program for calculating riser vortex induced oscillations and fatigue life. Testing tank facility, Massachusetts Institute of Technology, Cambridge, MA, USA.

[12] Vandiver, J.K. (2003). SHEAR7 User Guide. Department of Ocean Engineering, Massachusetts Institute of Technology, Cambridge, MA, USA.

CHAPTER II

MITIGATING FLOW-INDUCED VIBRATION OF A FLEXIBLE CIRCULAR CYLINDER VIA PRE-TENSION

Haoyang Cen, Mojtaba Ahmadi-Baloutaki, David S.-K. Ting, Rupp Carriveau

Turbulence and Energy Laboratory, Ed Lumley Centre for Engineering Innovation, University of Windsor, Ontario, Canada

H. Cen, M. Ahmadi-Baloutaki, D. S.-K. Ting, and R. Carriveau, "Mitigating flow-induced vibration of a flexible circular cylinder via pre-tension," *Sustainable Energy Technologies and Assessments*, in press.

Nomenclature

A	Cylinder's cross-sectional area	L	Cylinder's length
A_x	IL spatio-temporal response amplitude	m_s	Structural mass
A_y	CF spatio-temporal response amplitude	m^*	Mass ratio
CF	Cross-flow direction	Re	Reynolds number
D	Cylinder's outer diameter	T	Axial pre-tension
f_n	Fundamental natural frequency	U	Towing speed
f_x	IL vibration frequency	U_r	Reduced velocity
f_y	CF vibration frequency	ζ_s	Damping ratio
IL	In-line direction		

1 Introduction

Long flexible structures subject to water currents are a common occurrence in offshore engineering. The slender structures involved are prone to flow-induced vibration causing unnecessary motions and deflections which may result in structural fatigue or even premature failure if not properly mitigated. Therefore, it has driven particular interests of the oil industry for their engineering systems such as riser pipes, catenaries or mooring lines. Many other industries, for example offshore wind turbine and offshore energy storage, have also extended to this topic. It has been found that their susceptibility to flow-induced vibrations with high-coupled torsional, axial and lateral flexibility in deep water is able to induce higher harmonics in dynamics and vibration responses at frequencies higher than those caused by ocean waves [1]. In practical applications, to minimize deflections caused by drag force in the in-line (IL) direction that is transverse to the span, pre-tensions in the axial direction are commonly applied on cables and tethers. The applied pre-tensions may alter the natural frequency of cables and consequently affect their dominant harmonics of IL and cross-flow (CF) responses. Therefore, applying pre-tensions to cables and tethers is a potential way for active control of their underwater responses.

Among the published works investigating flow-induced vibrations of cylindrical structures in cross flows, the vast majority are on flexibly mounted short rigid cylinders with one or two degrees of freedoms [2−4]. In offshore energy and storage applications the structures involved are typically long and flexible, which tend to preclude benefitting from the vast historical research on simpler, short and rigid cylinders. More recently, however, with enhanced interest in deep water exploration some interesting work on the

slender flexible cylinders have been published [5, 6]. Systematic studies on the mitigation of severe flow-induced vibrations and failure through the use of pre-tension are still lacking.

Recently in a study by Chaplin *et al*. [7], a tensioned riser of 13.12 m in length and 28 mm in diameter, which resulted in an aspect ratio (cylinder's length/cylinder's outer diameter) of 468.5, was tested in step flow (35% of the model's length was submerged) over the Reynolds numbers range from 2500 to 25000. The mass ratio (mass of cylinder/mass of displaced fluid) of their model was about 3 and the bending stiffness was 29.9 $N \cdot m^2$. Five cases of axial tension (390 to 1925 N) were applied, resulting in five corresponding natural frequencies. Multi-modal response and structural modes up to the 8^{th} in cross-flow (CF), and 14^{th} in in-line (IL) direction were observed in this work. It was also reported that there was no relationship between the modes of vibration and the changes in pre-tension [7]. Following this experiment, Huera-Huarte and Bearman [8, 9] carried out a similar laboratory test on a vertical flexible cylinder with a diameter of 16 mm in step flow with Reynolds number between 1200 and 12000. Their model was 1.5 m long (L/D = 93.75) with a mass ratio of 1.8. Various pre-tensions in the range from 5 to 110 N were applied from the top end, giving fundamental natural frequencies from 3 to 7.1 Hz. The response of their model with lowest pre-tension was found to be similar to that of a flexibly mounted cylinder with well-defined initial, lower and upper branches within the lock-in region. At higher applied tension, however, only the initial and upper branches of response remained. This result is in contrast with the result from the study by Sanaati & Kato [1], in which clear initial, upper, lower and de-synchronization branches of response amplitude were shown. Sanaati & Kato [1] also found an increase of nearly

57% in lift coefficient and a decrease of about 30% in response amplitude as pre-tension increased from 73.5 to 294 N. Moreover, a narrowed lock-in bandwidth of response amplitude was observed with increasing pre-tension. In a study of a flexible cylinder with mass ratio of about 1 and pre-tension of 222.4 N, Lee & Allen [10] identified that if either one of the pre-tension and axial stiffness is large, the vibration frequency of a cylinder could significantly rise as flow speed increases.

Many discrepancies remain regarding the effect of pre-tension on flow-induced vibration of a flexible cylinder. This paper attempts to further study the effects of pre-tension on the dynamic response of a flexible cylinder with a relatively high aspect ratio and low mass ratio.

2 Experimental setup

The experiments were conducted in a 2.5 m long towing tank with a cross section of 0.8 × 0.8 m. The tank was filled with water up to a depth of 0.7 m. The towing motion is realized through the use of a pneumatic rod-less actuator and a supporting frame. As illustrated in Fig. 1a, the supporting frame employed to provide support for the flexible cylinder is firmly mounted under the actuator. Compressed air is applied to power the actuator with an effective travel distance of 1.6 m, during which the actuator would speed up rapidly from rest to steady speed, remaining steady over a short period before slowing down to rest again. The time consumed by acceleration and deceleration is around 0.8 s and 0.5 s respectively. Steady towing speeds from 0.1 to 1.6 m/s could be obtained by adjusting the compressed air pressure applied on the actuator. But in the present study, only speeds ranging from 0.1 to 0.8 m/s were investigated. In order to avoid resonance

response between the supporting frame and test cylinder, the frame is made highly rigid so that its natural frequency is well beyond that of the cylinder.

(*a*)

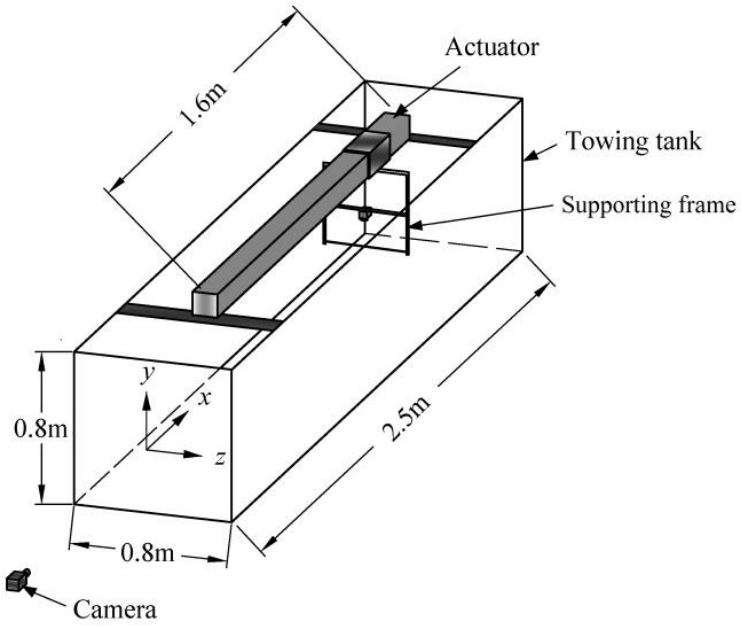

(*b*)

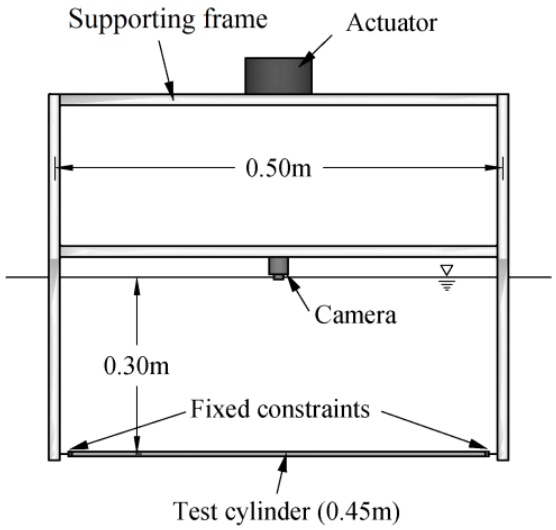

Fig. 1. Experimental setup: (*a*) A schematic of towing tank; (*b*) Supporting mechanism.

A Tygon tube with an effective length of 0.45 m was employed to provide a highly flexible model with low mass ratio of 0.77. The test model was a hollow cylinder

with inner diameter of 4.8 mm and outer diameter of 7.9 mm. Therefore, the aspect ratio (length to outer diameter) was 57 in this study. Two screws extending nearly 20 mm inside the cylinder were used as fixed constraints to make horizontal connection to the frame at both ends, as shown in Fig. 1b. With this pair of screws, the cylinder was sealed with air inside. Three end conditions with different axial pre-tensions, namely $T_1 = 0$, $T_2 = 4$, and $T_3 = 8$ N, were applied by means of adjusting the screws to stretch the cylinder. The pre-tensions were measured by a force meter through inducing same stretch on the cylinder before it was connected to the frame. Table 1 indicates their corresponding fundamental natural frequencies (frequencies of the first structural mode) and the symbols that represent the cases throughout this study. Impulse excitation tests were carried out to determine the fundamental natural frequencies and the damping ratios (damping coefficient/critical damping coefficient). As was found in our preliminary excitation tests, there were only small variations in the average value of damping ratios. The damping ratio is assumed to be constant in the current research. Based on the obtained fundamental natural frequencies, the reduced velocity, U_r (U/f_nD), was calculated to be in the range of 2 to 16. Details of the test model are summarized in Table 2. In order to minimize the impact of the free surface and boundary layer on the bottom of the tank, the test cylinder was located 0.40 m above the bottom surface and therefore 0.30 m beneath the static free surface, about 40 times its outer diameter.

Table 1. Pre-tension and corresponding natural frequency.

Pre-tension, T_n (N)	Symbol	Fundamental natural frequency (Hz)
0	□	5.16
4	Δ	7.15
8	o	9.14

To represent the phenomenon in a more realistic manner, the test cylinder was free to vibrate in both IL and CF directions with arbitrary amplitudes and stretch in the axial direction. For measurement of cylinder motions, two high-performance tracking cameras were employed at capture rates of 60 frames per second. One of them was positioned at one end of the tank for capturing the cylinder's cross-flow vibration while the other one was mounted above the cylinder for in-line motion. To avoid the impact of the free surface on image quality, the latter one was located slightly beneath the water surface. While the test is running, the mean drag force causes mean in-line displacement on the model. Consequently, the camera could not stay right above the cylinder during the test, leading to lowered accuracy. To minimize this effect, the camera mounted above the cylinder is positioned approximately 3*D* behind the cylinder in the IL direction.

Table 2. Test model characteristics and test parameters.

Aspect ratio	L/D	57
Axial stiffness	EA	120 N
Damping ratio	ζ_s	0.014
Flexural stiffness	EI	0.001 N·m^2
Length	L	450 mm
Mass	m_s	0.037 kg/m
Mass ratio	m^*	0.77
Outer diameter	D	7.9 mm
Reduced velocity	U_r	2~16
Reynolds number	Re	780~6300
Towing speed	U	0.1~0.8 m/s

Responses at three positions (identified as S1, S2 and S3) of the test cylinder were analyzed with the help of tracking cameras. The positions relative to the span of the model are 0.25, 0.5 and 0.75 of the cylinder length respectively, as illustrated in Fig. 2. The uniform cross-flow was generated by towing the test cylinder along the tank in calm water condition, and the time interval between two runs was set to be at least 10 minutes to minimize the disturbance caused by the previous run.

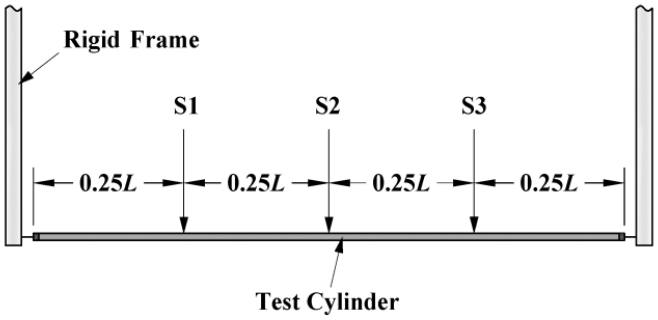

Fig. 2. Measurement positions along the model.

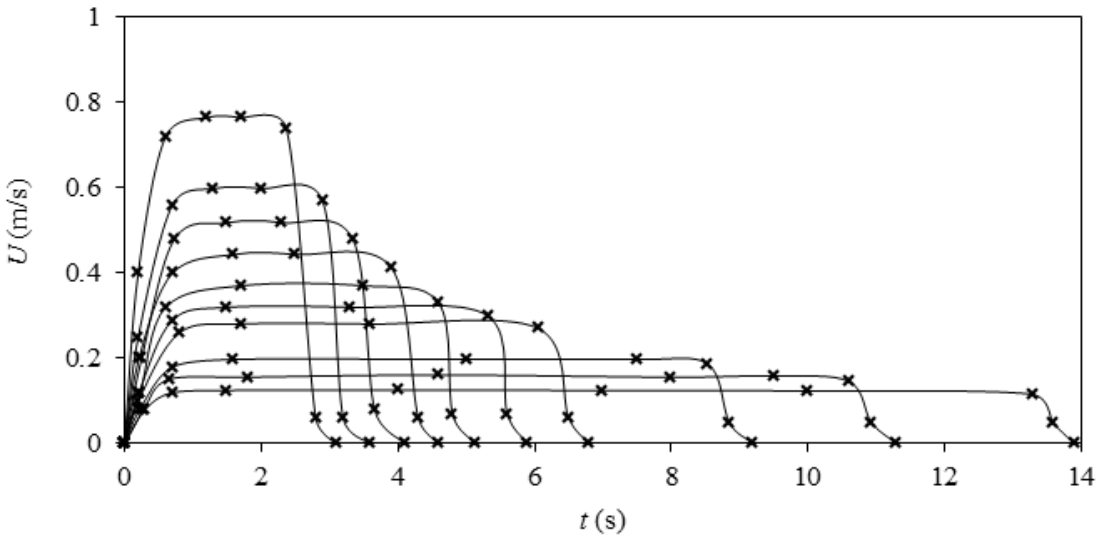

Fig. 3. Sample variation of towing speed.

Figure 3 shows the variation of the towing speed for the 4 N pre-tension case. It is clear that the towing carriage first accelerates rapidly for approximately 0.8 s before

reaching the steady towing speed followed by a rapid slowing down to rest. Obviously, higher steady towing speeds resulted in a quicker acceleration during the ramping-up stage. Note that there is about 12 s of constant velocity at the lowest towing speed while only around 0.5 s at the highest towing speed.

3 Result and discussion

In the present study, our focus has been on the dynamic response of a flexible model undergoing flow-induced vibration in order to obtain insights into underwater flexible cables' motion. Hence, in this section, the vibration amplitude and frequency are chosen to study the model's dynamic response. For all the following figures, symbols are used to indicate different pre-tension applied to the model as indicated in Table 1. For each run, the time window in which the model was being towed at a steady speed is used for performing vibration amplitude and frequency analysis. Though it is inevitable that the tension along the test model would increase due to the mean in-line displacement and therefore the natural frequency varies during the tests, the initial value of natural frequency is used for analysis and non-dimensionalizing the flow velocity according to

$$U_r = \frac{U}{f_n \cdot D} \tag{2.1}$$

where, f_n is the fundamental natural frequency of the test cylinder in still water obtained from impulse excitation test; D is the outer diameter of the cylinder. As shown in Fig. 1a, a Cartesian reference system is considered in this study and therefore IL response is denoted with $u(z, t)$ and CF one with $v(z, t)$. The vibration amplitude for both IL and CF

response are described with spatio-temporal standard deviations of responses, which are calculated as follows.

$$A_x = \sqrt{\frac{1}{s}\sum_{i=1}^{s}\left[\frac{1}{N}\sum_{j=1}^{N}\left[u_{ji}(z,t)-\overline{u_i}(z)\right]^2\right]} \tag{2.2}$$

$$A_y = \sqrt{\frac{1}{s}\sum_{i=1}^{s}\left[\frac{1}{N}\sum_{j=1}^{N}v_{ji}^2(z,t)\right]} \tag{2.3}$$

where, S is the number of time samples in the selected time window for analysis and N is the number of measurement positions. The uncertainties of vibration amplitude are estimated to be 10.3% for IL response and 8.9% for CF.

In Fig. 4, the dimensionless spatio-temporal standard deviations of the in-line and cross-flow displacements are presented. Initial, upper and lower branches of the response amplitude can be seen clearly for both IL and CF response. Differently, there are two peaks in IL response amplitude while only one in CF response amplitude. This is different from the findings of the study by Sanaati & Kato [1], where there were two peaks clearly shown for CF response amplitude. Clear initial upper branch and lower branch were also found in the study by Gu *et al*. [11] and Huera-Huarte and Bearman [8] at low pre-tension. However, Huera-Huarte and Bearman [8] only observed initial and upper branches at high pre-tension. In the present study, the first peaks of IL responses occur at a reduced velocity around 6, followed by the second peak around 10 for the case with pre-tension of 4 N, and 13 for the case with pre-tension of 0 N. It should be noted that although there is no implication of suppressing response amplitude, the obtained peak amplitude of response decreases with increasing pre-tension. Moreover, from the

plot of IL response amplitude, it can be seen that the lock-in bandwidth is narrowed as pre-tension increases, and this agrees with the findings of Sanaati & Kato [1].

(*a*)

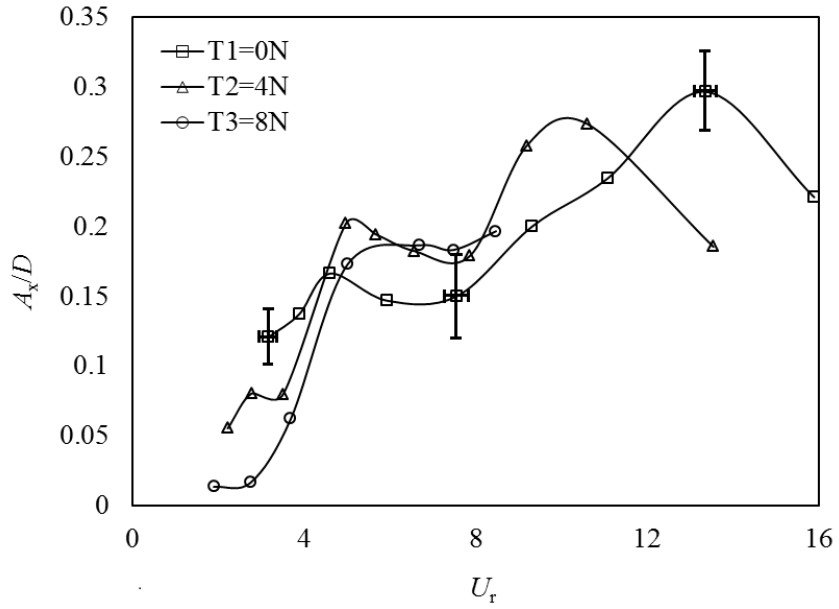

(*b*)

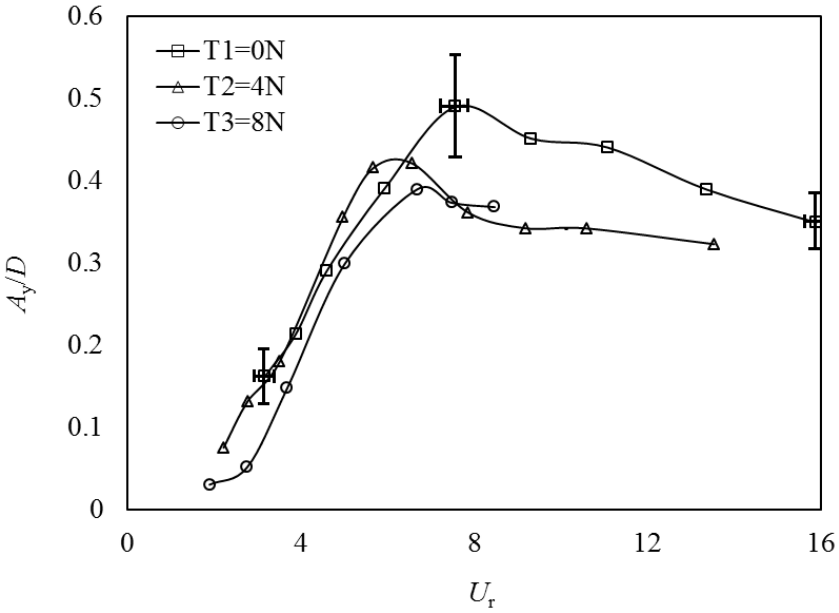

Fig. 4. Dimensionless amplitudes versus reduced velocity: (*a*) in-line (A_x^*/D); (*b*) cross-flow (A_y^*/D).

Dominant response frequencies that are the largest peaks in the spectra in each case were obtained by frequency analysis, using a Fast Fourier Transform of the response

amplitudes. In the IL response, the mean deflection due to mean drag force was removed from the response displacement in advance. Interestingly, the frequency ratios were found to be independent of the end conditions; though it was observed that with increasing pre-tension the response frequency increases.

(*a*)

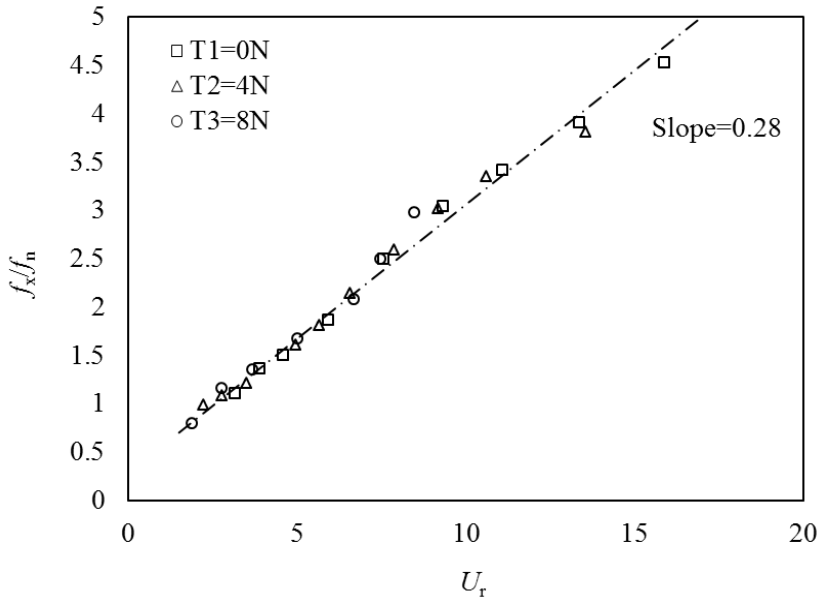

(*b*)

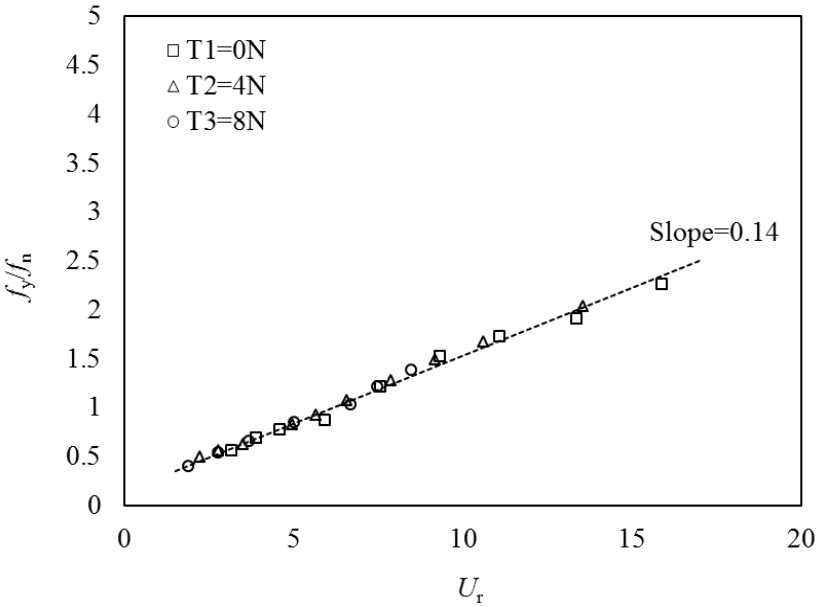

Fig. 5. Dimensionless response frequencies versus reduced velocity: (*a*) in-line (f_x/f_n); (*b*) cross-flow (f_y/f_n).

In Fig. 5, a linear fit to the data is also added to the frequency plot. The frequency ratio for IL and CF response for three end conditions remains linear with respect to the reduced velocity. The slope for IL response frequency in this work is 0.28 (see Fig. 5), which is between the values of 0.16 and 0.32 reported by Huera-Huarte and Bearman [8]. For CF response, the slope is 0.14 as can be observed in Fig. 5, slightly lower than the value of 0.16 found by Huera-Huarte and Bearman [8]. In a study by Gu *et al*. [11], IL response frequency was also observed to distribute into two branches with slope of 0.18 and 0.36 respectively, while the CF one was found to be 0.18. In the present study, the frequency ratio of IL to CF response is presented in Fig. 6. As expected, this ratio remains approximately around 2 with increasing reduced velocity despite the changes in end condition. This value was also reported by Sanaati & Kato [1] except for the IL lock-in and upper branch regions. Moreover, in the study by Gu *et al*. [11], the frequency ratio was found to be either around 1 or 2 when the reduced velocity is higher than 4.

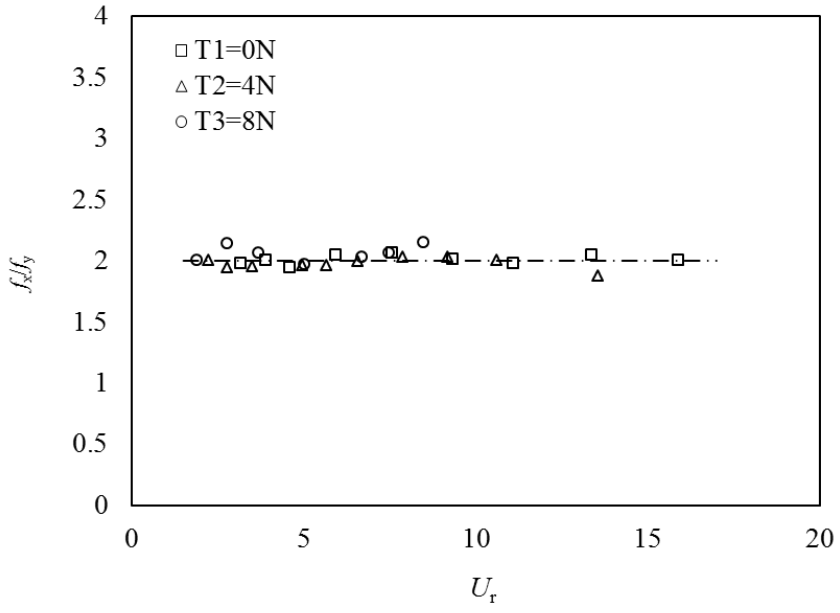

Fig. 6. Frequency ratio of in-line to cross-flow response versus reduced velocity.

4 Conclusion

An experimental investigation on the effects of pre-tension on hydrodynamic response of a highly flexible circular cylinder with 2 degree of freedom undergoing cross flow-induced vibration has been reported. The Reynolds number was varied from 780 to 6300 while the reduced velocity changed from 2 to 16. The response has been studied through vibration amplitude and frequency analysis. Three end conditions with pre-tension of 0, 4 and 8 N were tested. Within the tested tension range, two peaks were found in in-line response amplitude while only one in cross-flow response. With increasing pre-tension, the amplitude of vibration, especially the cross stream one, appeared to decrease. This is particularly the case at reduced velocity corresponding to the maximum vibration amplitude. Moreover, pre-tension seems to be able to narrow the lock-in bandwidth in in-line response. Also examined was the vibration frequency. Independence of pre-tension was shown in frequency ratios. For frequencies ratios of IL and CF response to fundamental natural frequencies, with increasing reduced velocity, they increased approximately linearly with the tested range. The slopes of linear fitting are 0.28 and 0.14 for IL and CF motions respectively. The ratio of IL response frequency to CF one remained at approximately 2 within the tested range despite the changes in pre-tension. It should be noted that the pre-tension range tested in this study was relatively narrow so the effects of pre-tension on suppressing vibration amplitude cannot be generalized. Further study with wider pre-tension ranges is needed to achieve a more comprehensive understanding of the effects of pre-tension on flow-induced vibration of flexible cylinder.

Acknowledgement

This work is made possible by Natural Sciences and Engineering Research Council of Canada.

References

[1] Sanaati, B., & Kato, N. (2012). A study on the effects of axial stiffness and pre-tension on VIV dynamics of a flexible cylinder in uniform cross-flow. *Applied Ocean Research*, **37**, 198–210.

[2] Bearman, P.W. (1984). Vortex shedding from oscillating bluff bodies. *Annual Review of Fluid Mechanics*, **16**(1), 195–222.

[3] Sarpkaya, T. (2004). A critical review of the intrinsic nature of vortex-induced vibrations. *Journal of Fluids and Structures*, **19**(4), 389–447.

[4] Williamson, C.H.K., & Govardhan, R. (2004). Vortex-induced vibrations. *Annual Review of Fluid Mechanics*, **36**, 413–455.

[5] Blevins, R.D. (2001). Flow induced vibrations. Second Edition, Krieger Publishing Company, Malabar, Florida, USA.

[6] Vandiver, J.K. (1993). Dimensionless parameters important to the prediction of vortex-induced vibration of long, flexible cylinders in ocean currents. *Journal of Fluids and Structures*, **7**(5), 423–455.

[7] Chaplin, J.R., Bearman, P.W., Huarte, F.H., & Pattenden, R.J. (2005). Laboratory measurements of vortex-induced vibrations of a vertical tension riser in a stepped current. *Journal of Fluids and Structures*, **21**(1), 3–24.

[8] Huera-Huarte, F.J., & Bearman, P.W. (2009). Wake structures and vortex-induced vibrations of a long flexible cylinder–part 1: dynamic response. *Journal of Fluids and Structures*, **25**(6), 969–990.

[9] Huera-Huarte, F.J., & Bearman, P.W. (2009). Wake structures and vortex-induced vibrations of a long flexible cylinder–part 2: drag coefficients and vortex modes. *Journal of Fluids and Structures*, **25**(6), 991–1006.

[10] Lee, L., & Allen, D. (2010). Vibration frequency and lock-in bandwidth of tensioned, flexible cylinders experiencing vortex shedding. *Journal of Fluids and Structures*, **26**(4), 602–610.

[11] Gu, J., Vitola, M., Coelho, J., Pinto, W., Duan, M., & Levi, C. (2013). An experimental investigation by towing tank on VIV of a long flexible cylinder for deepwater riser application. *Journal of Marine Science and Technology*, **18**(3), 358–369.

CHAPTER III

EFFECT OF MASS RATIO ON THE HYDRODYNAMIC RESPONSE OF A FLEXIBLE CYLINDER

Haoyang Cen, Rupp Carriveau, and David S-K. Ting

Turbulence and Energy Laboratory, Ed Lumley Centre for Engineering Innovation, University of Windsor, Ontario, Canada

Under review for publication in Journal of Marine Science and Application

Nomenclature

A	Cylinder's cross-sectional area	L	Cylinder's length
A_x	IL spatio-temporal response amplitude	m_s	Structural mass
A_y	CF spatio-temporal response amplitude	m^*	Mass ratio
CF	Cross-flow direction	Re	Reynolds number
D	Cylinder's outer diameter	T	Axial pre-tension
f_n	Fundamental natural frequency	U	Towing speed
f_x	IL vibration frequency	U_r	Reduced velocity
f_y	CF vibration frequency	ζ_s	Damping ratio
IL	In-line direction		

1 Introduction

The dynamics of cylindrical structures subjected to cross flow have received a great deal of attention. This to a great extent is because of their engineering importance, particularly in offshore engineering where they are extensively deployed in cross flow as deep water exploration pipes, oil production risers, catenaries etc. Inevitably external forces exerted by the nearby fluid flow cause these cylindrical structures to oscillate, in both stream-wise (in-line, IL) and transverse (cross-flow, CF) directions. This phenomenon is termed as flow-induced vibration (FIV) [1]. Increasing the dynamic load on offshore structures, FIV could be a significant source of fatigue damage or even premature failure. Hence, a comprehensive understanding of the underlying dynamic interaction mechanism is important such that general prediction of occurrence, as well as probable response amplitude and frequency, corresponding approaches for mitigation could be established for offshore engineering designs.

1.1 Elastically mounted rigid circular cylinders

Research in this field began with elastically mounted rigid cylinders with one or two degrees of freedom (1DF or 2DF). Fundamental characteristics like dynamic forces, vortex shedding mode, lock-in region, effects of surface roughness and mass ratio, have driven most interests. The current state of the field and comprehensive reviews are provided in [2–8] among others. Review of these references suggests that in terms of a cylinder's dynamic response, mass ratio is an influential parameter. It is well recognized that a rigid cylinder's amplitude response is classified into three main categories, depending on the value of mass ratio (see Fig. 1). Firstly, a cylinder with high mass ratio

vibrating in cross-flow direction typically displays two branches of response amplitude, namely the 'initial' and 'lower'. This was first reported in a study with mass ratio of 248 by Feng [9]. An abrupt jump and hysteretic transition between these two branches was also presented. The jump in response amplitude was accompanied with a jump in the phase of pressure fluctuation, which was later revealed to be associated with a transition in wake pattern, from the '2S' mode (2 single vortices shed per cycle, Fig. 2a) to '2P' (2 vortex pairs shed per cycle, Fig. 2b), i.e., '2S' corresponded to the initial branch while '2P' to the lower one [10–12].

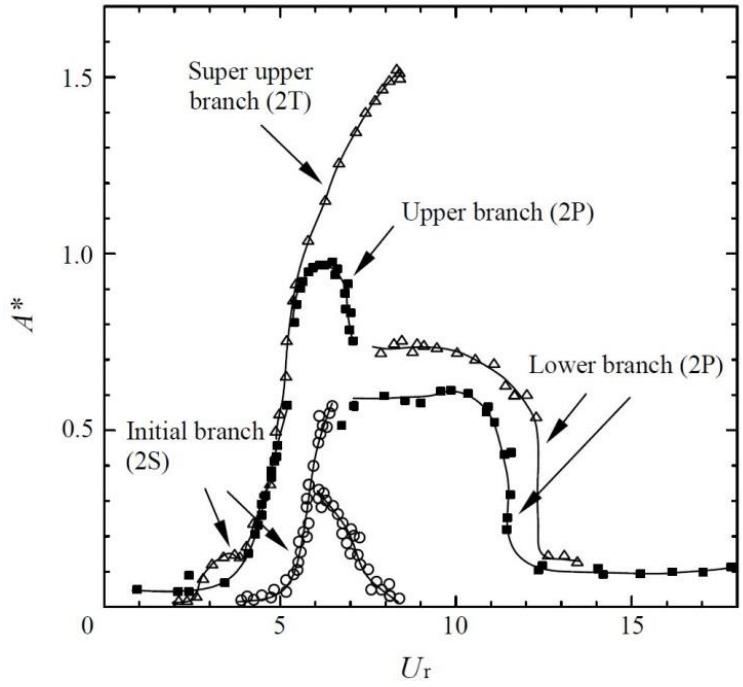

Fig. 1. Cross-flow vibration amplitude (A^*) of an elastically mounted cylinder versus reduced velocity, U_r, demonstrating various branches and corresponding vortex shedding mode: data from Feng [9] at mass ratio, $m^* = 248$ (open circle symbols); Khalak & Williamson [13] at $m^* = 2.4$ (solid square symbols); and Jauvtis & Williamson [14] at $m^* = 2.6$ (open triangle symbols).

An elastically mounted cylinder with reduced mass ratio would experience increases in its amplitude response [15]. Further to this, a new branch, namely the 'upper' branch, was discovered between the initial and lower branches with large response amplitude [12, 13, 16, & 17]. A new vortex shedding mode similar to the '2P' mode, with two vortex pairs shedding per cycle but the latter vortices of each pair significantly weaker than the first (Fig. 2c), was revealed to correspond to the 'upper' branch. Beyond this, low mass ratios also make the added mass comparable to cylinder's structural mass, which includes any enclosed matter but excludes the hydrodynamic mass. This results in a non-negligible variation in the total mass and would thus alter the natural frequency. Consequently, significantly broader lock-in regions, within which the vortex shedding frequency departs from the *Strouhal* frequency and synchronizes with the natural frequency, is common when the vibrating cylinder has low mass ratios [15].

Further investigation on rigid cylinders was extended to 2DF by Jauvtis & Williamson [14, 18, & 19]. They carried out a comprehensive study on a rigid cylinder permitted to oscillate in in-line and cross-flow directions, in which the cylinder was designed to have identical natural frequencies and mass ratios ranging from 1.5 to 25.0. The added freedom in the in-line direction was found to have little influence on the cross-flow vibration at high mass ratio, i.e., the findings from 1DF scenarios remained of strong relevance to the case of 2DF. The influence became more evident as the mass ratio decreased. They concluded that in the cases of mass ratios above five or six, the added freedom had limited influence on the cross-flow response; however, once mass ratio fell below this value, the system's response was drastically modified: the upper branch was replaced by a new branch (denoted as 'super upper'; see Fig. 1) characterized by 1.5

diameters amplitude and '2T' vortex shedding mode that comprised a triplet of vortices every half cycle (Fig. 2d). This trend persisted until it reached the critical mass ratio of around 0.54, below which large amplitude vibration persisted over the tested range above initial lock-in.

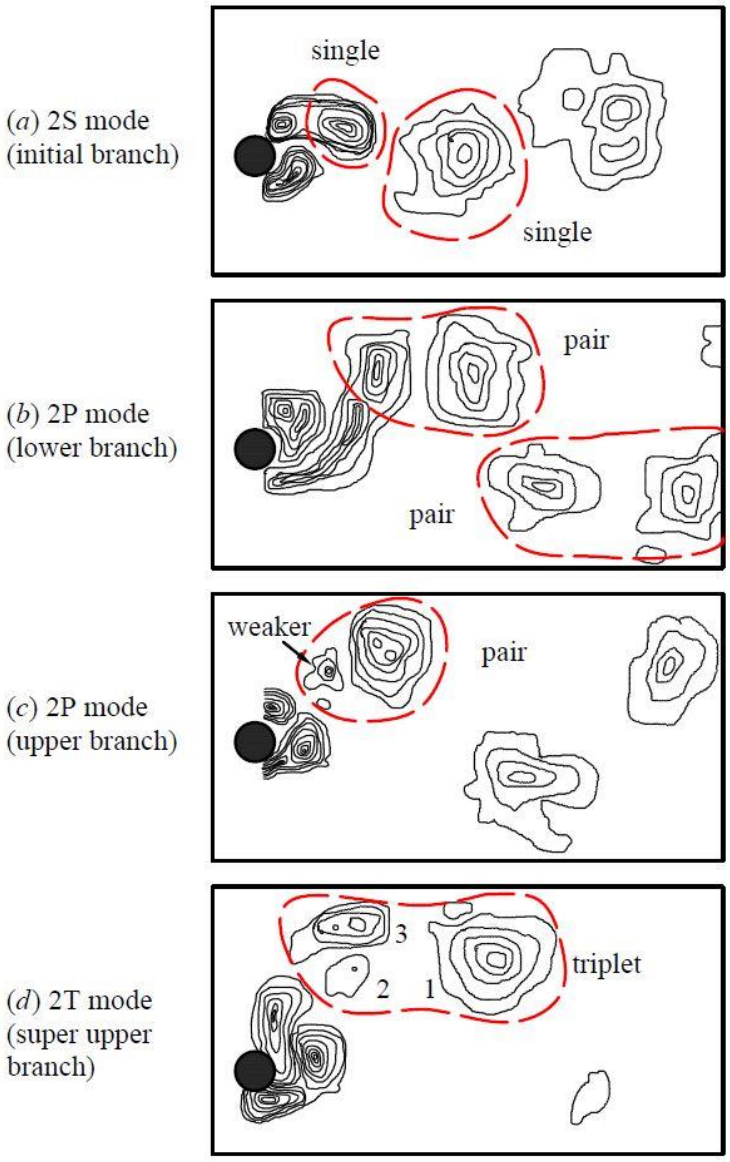

Fig. 2. Vortex shedding modes of an elastically mounted cylinder: (a), (b) and (c) shows the modes corresponding to the initial, lower and upper branches respectively from [12]; (d) shows the mode corresponding to the super upper branch, from [18, 19].

1.2 Flexible circular cylinders

With the extensive use of flexible cylinders in offshore engineering, studies on FIV have been extended to flexible cylinders in recent decades, but it has not been covered as extensively as rigid cylinders. The structural flexibility introduces a capacity of vibrating at high modes. When this is considered concurrently with their added mass and damping distribution while in motion, it results in added complexities like single/multi-mode vibration and thus multi-frequency, modes competition, traveling waves along the cylinders' length etc. [20–23]. For a vibrating flexible cylinder, the cable-like and beam-like structures are two generally accepted structural systems for analysis. It is termed a cable if the tension dominates, while it is termed a beam if the bending rigidity does. Results from the study by Lee and Allen [24] showed that the vibration frequency of a cylinder rises with the flow speed for a tension-dominated structure but does not rise significantly for a bending rigidity dominated structure. In addition, the lock-in bandwidth is broad for bending-dominated cases, indicating a weak association between the changes in vibration frequency and lock-in bandwidth.

In a pioneering work involving flexible cylinders by Vandiver [25] experimental results from previous research on flexible cylinders were consolidated to reveal the non-dimensional parameters governing the phenomena of VIV in flexible cylinders. The significance of mass ratio was again emphasized. It was indicated that cylinders with low mass ratios present a broader lock-in range than those with high mass ratios, a fact also observed in rigid cylinder studies. However, due to the challenges in varying a mass ratio during a set of tests for a constructed, instrumented flexible cylinder, a systematic study to ascertain the dependence of the cylinder's dynamic response on mass ratio is still rare.

Chaplin *et al*. [26] carried out a set of laboratory tests on a tensioned riser with an aspect ratio of 468.5, a mass ratio of about 3, done in step flow (35% of the cylinder's length was submerged). Cross-flow vibration modes up to the 8th were observed as well as multi-mode responses. Contributions from several modes were found in the responses at all reduced velocities but the lower ones. Huera-Huarte & Bearman [27] carried out a similar test on a flexible cylinder with an aspect ratio of 94 and a mass ratio of 1.8. The maximum attainable amplitudes up to about 0.7 diameters in the cross-flow direction and 0.3 diameters in-line were reported. This was considered a difference from the flexibly mounted rigid cylinder, where response amplitude over 1.5 diameters was demonstrated in a study by Jauvtis & Williamson [14]. The response frequencies in lock-in region were found to synchronize with the natural frequency of the responding mode. They reported using a *Strouhal* number of about 0.16 to predict the response frequencies as Chaplin *et al*. [28] proposed in the past.

Working in line with their studies, Huera-Huarte *et al*. [29] recently reported a new response data set on a flexible cylinder. They presented the dynamic response of two slightly different flexible cylinders: one with a mass ratio and aspect ratio of 1.1 and 158 respectively while the other one of 2.7 and 187. They reached a conclusion that very low mass ratio had the effect of leading to a large increase in both cross-flow and in-line response amplitude on flexible cylinders, similar to what it had on elastically mounted rigid cylinders. Besides, the overall response in very low mass ratios appeared to be contributed from a larger number of modes. Unfortunately no direct comparison was made in the dynamic responses between the two cylinders due to the fact that those two cylinders were not practically identical except for the mass ratio. To the best of the

authors' knowledge, this is the only experimental work in the literature involving flexible cylinders with different mass ratios. More research efforts and systematic investigation on the effect of mass ratio are required.

For the present work a series of experimental tests have been carried out to further investigate the flow-induced vibration of a highly flexible circular cylinder at especially low mass ratios. The focus is on revealing whether varying mass ratios, below 6, would cause significant variations on overall response mode, amplitude and frequency. Measurements are obtained for the cylinder's response to vortex excitation at high modes in both cross flow and in line directions.

2 Description of the experiment

2.1 Towing tank

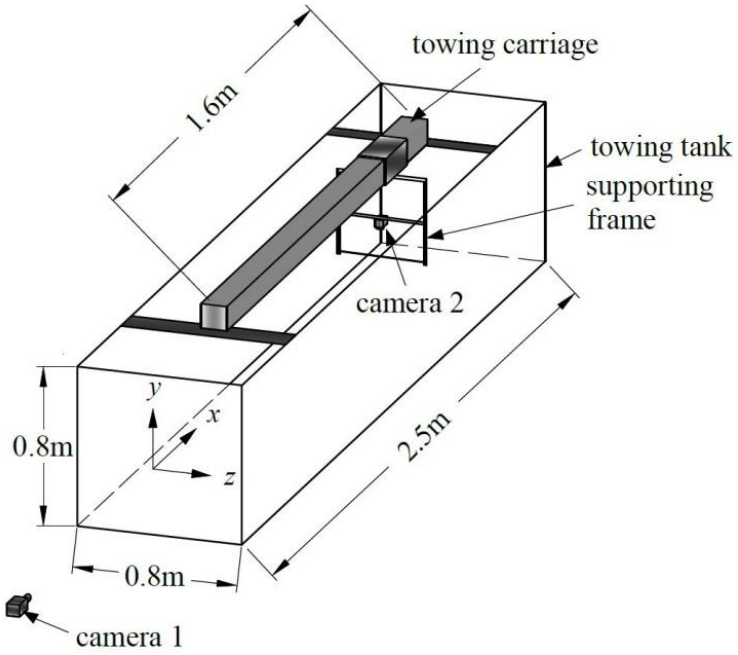

Fig. 3. Sketch of overall experiment setup.

The towing tank utilized was located in the Turbulence and Energy Laboratory at the University of Windsor. Made of glass, it is a transparent tank with dimensions of 2.5 × 0.8 × 0.8 m (see Fig. 3). During the tests, it was filled with water up to a depth of 0.7 m. Its transparency made the optical access possible.

The overall experimental configuration is illustrated in Fig. 3. A pneumatic rod-less actuator was installed and fixed horizontally along the tank's length, in the centre of the tank width span. It drives a rigid frame that serves as the towing carriage. The rigid frame is mounted firmly under the actuator. The rigid frame itself introduces a high natural frequency that is well beyond that of the cylinder; which ideally does not interfere with its response. The horizontal connection of the test model to the rigid frame is achieved through fixed constraints, which are a pair of set screws, at both ends, elevating the cylinder at a height of 400 mm from the tank's bottom, so there is 300 mm between the cylinder and the free surface. According to a numerical study of fluid flow past a circular cylinder by Farrant *et al*. [30] it is reasonable to neglect both the effects of tank bottom and free surface at such distances, as they are around 50 and 40 times the cylinder's diameter. While horizontally holding the test cylinder, this pair of screws extended approximately 15 mm into the cylinder in its axial direction and therefore also acted as two plugs at its ends to help seal the cylinder with desired materials inside. This towing apparatus carries the test cylinders through still fluids over a total travel distance of 1.6 m. During the travel distance, the carriage accelerates rapidly from rest to a constant testing velocity and back to rest again. The speed of the carriage is pressure-controlled, i.e., by adjusting the applied pressure on the actuator, towing speeds up to 1.6 m/s are possible.

2.2 Characteristics of the flexible cylinder

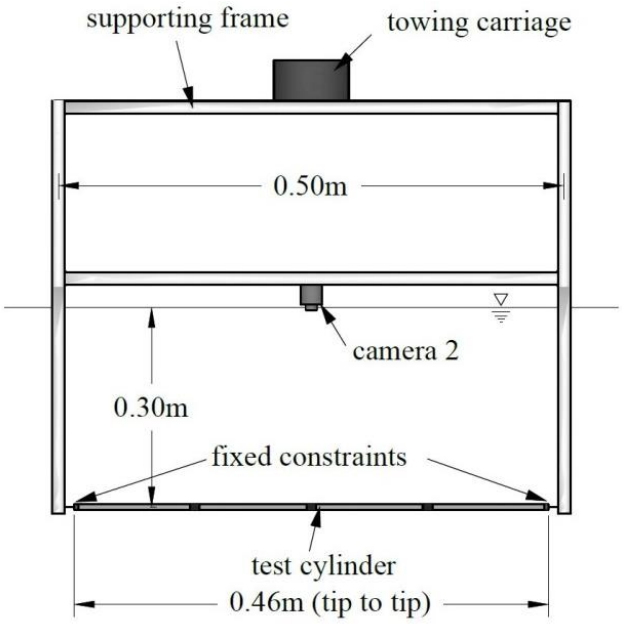

Fig. 4. Supporting mechanism.

The flexible circular cylinder tested is a hollow Tygon tube with an inner diameter of 4.8 mm (3/16 in.) and outer diameter of 7.9 mm (5/16 in.). It has an initial length of 420 mm and is horizontally connected to the rigid supporting frame via a set of screws at both ends, as shown in Fig. 4. It should be noted that the tip to tip distance between the two screws is 460 mm (effective length), i.e., the flexible cylinder reaches a tensioned state (40 mm elongation) when installed in place. From this point forward, the cylinder's length will always refer to the effective length (460 mm). Inevitably a reduction in the cylinder's diameter occurs when it is being stretched. Measurements were conducted on the stretched cylinder's outer diameter using a digital caliper and it was found to be around 7.91 mm, based on which the reduction rate is calculated to be 3%. Since it is not remarkable, the cylinder's outer diameter is considered as 7.9 mm throughout the whole study. Therefore the test cylinder's aspect ratio, which is defined as

ratio of length to outer diameter, is 58 in the present study. The axial pre-tension applied on the stretched cylinder was measured to be around 11 N, using a force meter by means of inducing identical elongation (40 mm) on the cylinder when it was disconnected from the supporting frame. For the convenience of comparison with literature, the value of pre-tension is converted to a dimensionless form of 1200, using

$$T^* = T / T_{cr} \tag{3.1}$$

where, T is the pre-tension, and T_{cr} is the critical compression load for buckling. T_{cr} can be obtained from

$$T_{cr} = \pi^2 EI / 4L^2 \tag{3.2}$$

where, E is the Young's modulus of the model material, I the cross-sectional inertia and L the model's original length. The high value of dimensionless pre-tension is mainly a result from the low critical compression load. In the present study, the cylinder is towed through the water in speeds ranging from about 0.1 m/s to 1.6 m/s. Accordingly, the Reynolds number based on its diameter spans from 800 to 13,000 while reduced velocities range from 1 to 25, calculated from

$$U_r = \frac{U}{f_n \cdot D} \tag{3.3}$$

where, U is the towing speed; f_n is the natural frequency of test cylinder in its first vibration mode; D is the cylinder's outer diameter. It should be noted that f_n will be altered as the result of the varying mass ratio. Therefore, cases with different mass ratio may have different value of U_r at a same towing speed. To maintain a uniform cross flow at least 10 minutes are taken as time interval between runs for minimizing the disturbance

induced by previous run. The cylinder's material properties and tested flow conditions are summarized in Table 1.

Table 1. Cylinder material properties and flow conditions.

Aspect ratio	L/D	58
Axial stiffness	EA	124 N
Effective length	L	460 mm
Flexural stiffness	EI	0.001 N·m^2
Mass	m_s	37 g/m
Outer diameter	D	7.9 mm
Pre-tension	T^*	1200
Reduced velocity	U_r	2 − 25
Reynolds number	Re	800 − 13,000
Towing speed	U	0.1 − 1.6 m/s

Table 2. Test cases with corresponding parameters.

Mass ratio	Designation	Fill material	Material density	Fund. nat. freq.	Damping ratio
0.7	M-0.7	Air	1.2 kg/m^3	11.3 Hz	4%
1.0	M-1.0	Water	997.1 kg/m^3	10.3 Hz	3%
3.4	M-3.4	Alloy powder	8000 kg/m^3	8.4 Hz	3%

As our focus of this study is the effect of mass ratio on the cylinder's flow-induced vibration, the cylinder is pre-pared to have different mass ratios by filling the cylinder with different materials. Mass ratios of flexible structures in offshore applications can be as low as 3 [29], and as noted there is a dearth of investigations for mass ratios near 1. Subsequently, the mass ratios in the present study were chosen to explore low values, namely 0.7, 1.0 and 3.4. These were achieved by filling the cylinder

with air, water and alloy powder respectively. Table 2 indicates the fill materials and each case's fundamental natural frequency (natural frequency of the first structural mode) as well as damping ratio (damping coefficient/critical damping coefficient) in still water. Fundamental natural frequency and damping ratio for each case was determined via free decay test where impulse excitation was imposed to the mid-span of the tensioned cylinder. This was achieved by slightly flipping the submerged cylinder's mid-point using a slim iron wire. The midpoint's response was then captured and analyzed using fast Fourier transform (FFT). The time history and spectra of case M-3.4's midpoint during decay test is presented in Fig. 5 as an example. Damping ratio was determined via logarithmic decrement from

$$\zeta = \frac{\ln(y_n / y_{n+m})}{2\pi \cdot m} \tag{3.4}$$

where, y_n is the displacement of the n^{th} cycle, and y^{n+m} of the $(n+m)^{th}$ cycle. As found from the tests, the case with air has a damping ratio of 4%, which is 1% higher than that of cases with water and alloy powder.

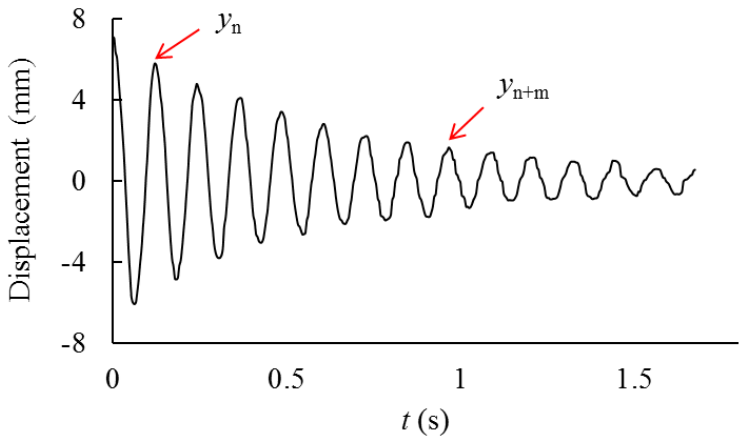

Fig. 5. Time history of decay test (alloy powder).

2.3 Measurement technique

In the present study, the response of the flexible cylinder was measured optically. Two high-speed cameras were deployed to track its vibration response at a rate of 240 frames per second. As illustrated in Fig. 3, to visualize the cross flow response, Camera 1 was installed at one end of the tank, 10 m from the cylinder's initial position, horizontally aligned with the test cylinder. Camera 2 was mounted above the cylinder on the supporting frame for the in-line response measurement (also illustrated in Fig. 4). During tests, Camera 2 was carried through the fluids and thus stayed above the model. To eliminate the impact of free surface on video quality, Camera 2 was immersed slightly beneath the water surface. While the test is running, the mean drag force causes mean in-line displacement on the model. Consequently, the camera could not stay right above the cylinder during the test, leading to lowered accuracy. To minimize this effect, Camera 2 was positioned approximately 3*D* behind the cylinder's initial position in the IL direction. Marking three locations of the cylinder span, 8 mm wide fluorescent tape rings served as a visualizing target, as shown in Fig. 6. Identified as S-0.25, S-0.50 and S-0.75, their relative positions on the model's span are 0.25, 0.50 and 0.75 respectively.

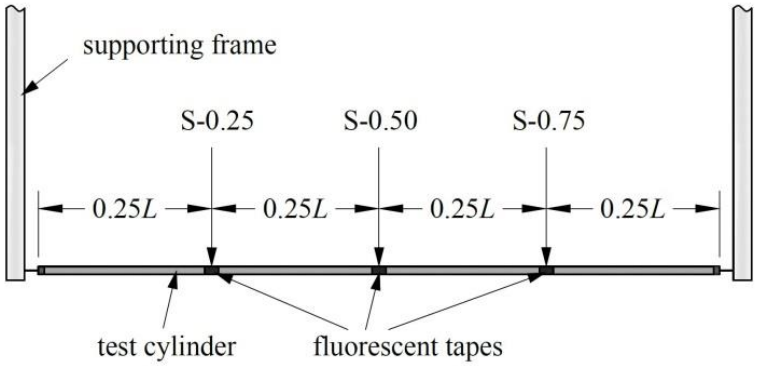

Fig. 6. Measurement locations and their designations.

3 Result and discussion

The hydrodynamic response of a flexible cylinder is a nonlinear phenomenon and is highly dependent on parameters such as reduced velocity, Reynolds number, mass ratio and damping ratio. Many studies have attempted to combine mass ratio and damping ratio to investigate the cylinder's response. As the damping ratios of three tested cases in the present study are nearly the same (4%, 3% and 3%), it is now assumed that the small variation in damping ratio has little influence on the cylinder's response. Consequently, the variation in mass ratio is deemed to be the major contributor to the difference in system's response.

A Cartesian reference system with origin at the mid-span of the model as shown in Fig. 3 is under consideration in the present study, with x denoting the in-line direction, y the cross-flow and z the span-wise. Therefore, $u(z, t)$ and $v(z, t)$ are used to represent the instantaneous displacements in the in-line and cross-flow directions respectively.

3.1 Towing motion and resulted response

As mentioned above, the towing carriage is actuated by compressed air starting from rest and advancing to a constant velocity. After a short period of that it decelerates to a complete stop. This towing motion is demonstrated in Fig. 7, showing several cases' time histories of the towing speeds as examples. It is noted that the positive and negative acceleration stages consume approximately 0.8 s and 1 s respectively for all the speeds. Hence, the time period remaining for constant speed motion is approximately 12 s for the lowest towing speed of 0.1 m/s and 0.6 s for the highest speed of 1.6 m/s.

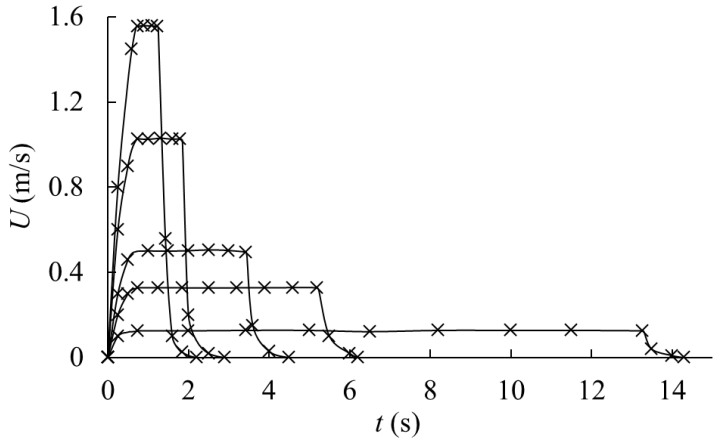

Fig. 7. Examples of time history of towing speed.

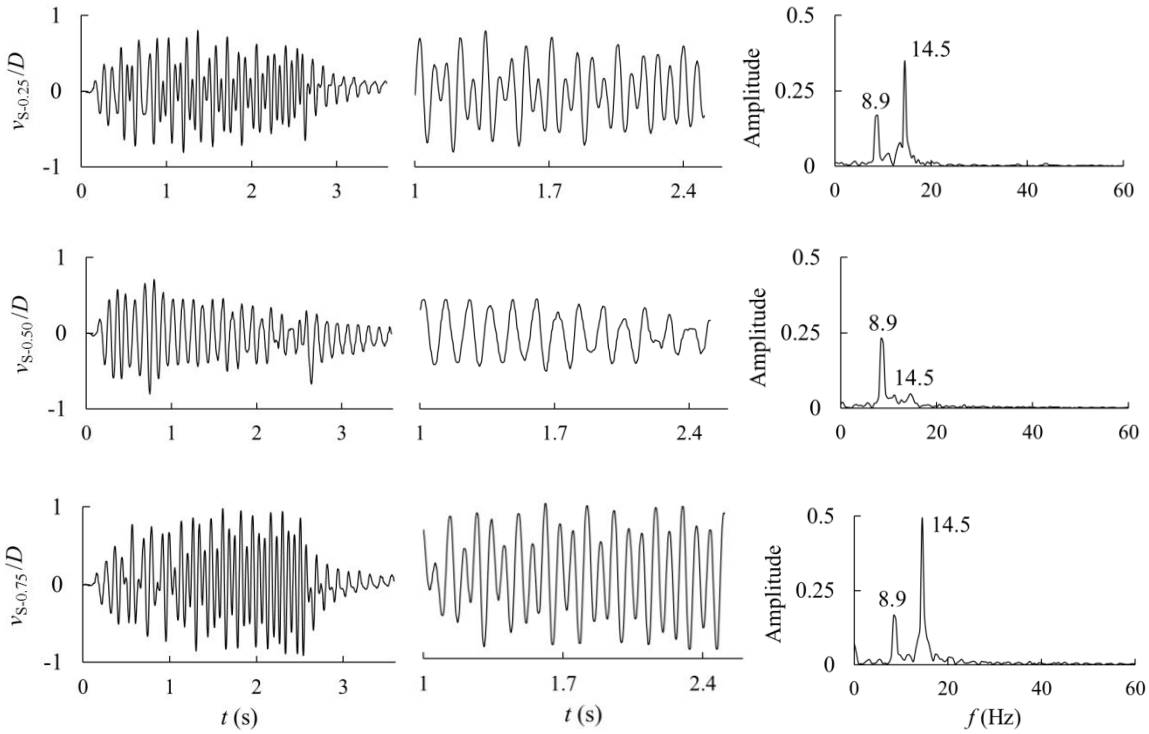

Fig. 8. History of CF displacement, and corresponding amplitude spectra for case M-3.4 at U = 0.53 m/s

The variance in towing speed is also reflected in the left column of Fig. 8, showing the time history and corresponding spectra of the cross-flow response displacement for the case M-3.4 at a towing speed of 0.53 m/s. The cylinder becomes

excited as the towing carriage is actuated, and experiences rapid increase in response amplitude until around 0.8 s. Steady vibration appears to be reached approximately at a time of 1 s. Finally at $t \approx 2.5$ s, a drastic change in the displacement is seen, reflecting the sharp slowdown of the towing carriage. To study the cylinder's hydrodynamic response through the steady vibration stage, a time window, within which the cylinder vibrates steadily, is thus applied to each case to select data of interest. Only displacement within the time window is processed for vibration amplitude and frequency analysis. The mid-column of Fig. 8 presents the enlarged time histories of displacement in these chosen time intervals [1, 2.5] s. FFT is thereafter applied to the selected data to obtain the spectra distribution, which is demonstrated in the right column of Fig. 8.

3.2 Multi-frequency vibration & higher harmonics

One can see from the right column of Fig. 8 that there are two distinct peaks at frequencies of 8.9 and 14.5 Hz, indicating significant contributions from these two frequencies in the cylinder's cross-flow response. Furthermore, the dominant frequency, which has the highest peak in the spectra, is found to be different at locations along its span. In the case shown in Fig. 8 for example, its mid-span, S-0.50, is dominated by frequency of 8.9 Hz, while S-0.25 and S-0.75 dominated by frequency of 14.5 Hz. This could suggest that the cylinder is undergoing multi-frequency vibration with different span locations vibrating at different frequencies. It should be noted that this is not a special case in the cylinder's dynamic response; it also appears at other towing speeds and in cases M-0.7 and M-1.0.

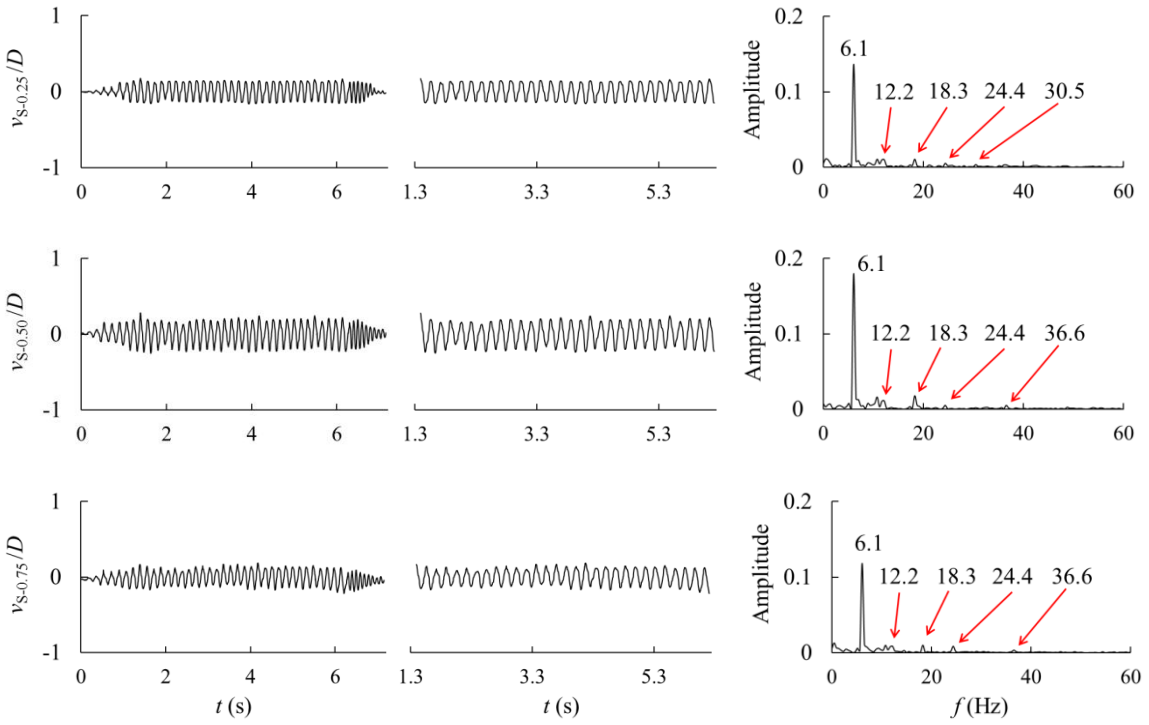

Fig. 9. History of CF displacement, and corresponding amplitude spectra for the case M-1.0 at U = 0.24 m/s.

Another common phenomenon is that the outstanding frequencies are found to be in fold-increase in some tested cases' response spectra. For example, Fig. 9 shows the dis-placement and spectra of case M-1.0 at U = 0.24 m/s in a fashion similar to Fig. 8. A dominant vibration frequency of 6.1 Hz is outstanding over the range. In addition to that, notable contributions from frequencies that are 2, 3, 4, 5, and 6 times the dominant one are also identified in its dynamic response, indicating the existence of higher harmonics. This might be a result from the synchronization between the vortex shedding frequency and the vibration frequency. For an underwater circular cylinder the vortex shedding frequency follows *Strouhal* frequency (f_{st}) when lock-in is not present. According to Figs. 14 & 15 that present the response amplitudes of in-line and cross-flow vibrations, it is clear that lock-in is absent for case M-1.0 at U = 0.24 m/s (U_r = 2.9). Hence, it is

reasonable to assume the vortex shedding frequency (f_v) for the case under consideration follows the *Strouhal* frequency, i.e., $f_v = f_{st}$. Then we evaluate the vortex shedding frequency, as

$$f_{st} = St \cdot (U / D) \tag{3.5}$$

by adopting $St = 0.2$, a value of 6.07 Hz is identified for f_{st} and thus f_v at $U = 0.24$ m/s. That means the higher harmonics are associated with the synchronization between vortex shedding and vibration frequencies. Unlike the higher harmonics reported by Vandiver *et al*. [31] and Song *et al*. [32], which only had the odd multiple harmonics in cross-flow response, both odd and even multiples are found in the cross-flow response in the present study. As suggested by Song *et al*. [32], higher harmonics require more design attention since their high frequencies likely lead to more severe fatigue damage.

3.3 General vibration characteristics

Figure 10 demonstrates the response spectra at S-0.50 of three cases expressed with respect to reduced velocity. The left column shows the spectra of in-line response, while the right column shows that of cross-flow response. One can see from the in-line spectra that for case M-0.7, which has air sealed inside the cylinder, its vibration frequency increases nearly linearly with increasing reduced velocity, similar to that of a rigid cylinder. Govardhan & Williamson [12] reported a relation close to linear between the vibration frequency and current velocity on the cylinder with $m^* \approx 1$. The highest frequency observed in current study is around 60 Hz. It is also clear that at a reduced velocity around 6, the cylinder experiences a significant amplitude peak. Similarly for case M-1.0, its vibration frequency also rises as reduced velocity increases and reaches an

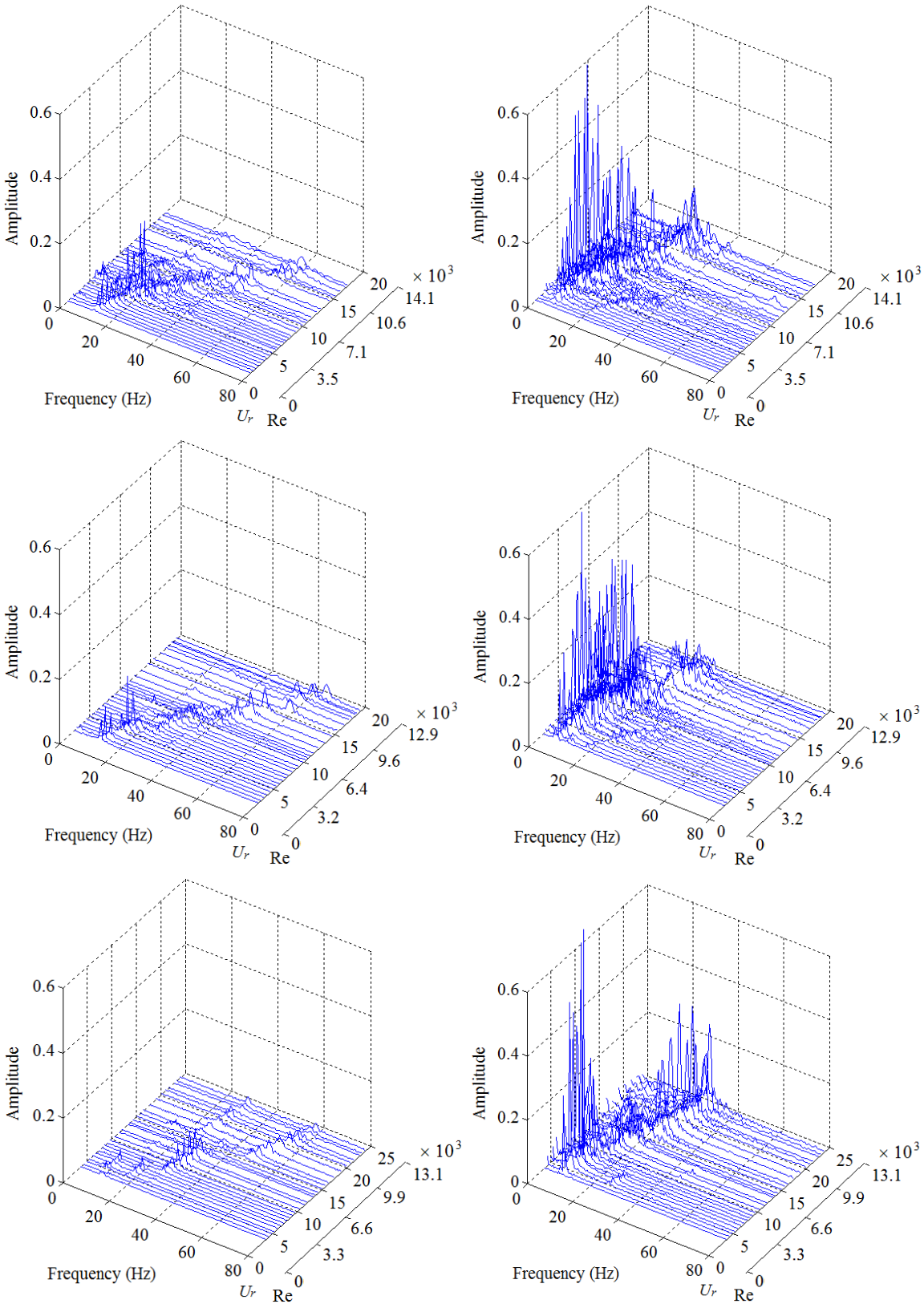

Fig. 10. Spectral distribution of S-0.50: from top to bottom are M-0.7, M-1.0, M-3.4 with left column for IL response, right for CF.

amplitude peak at $U_r \approx 6$. However, it is noticeable that at reduced velocity around 7, there is a sudden change in the vibration frequency of case M-1.0, jumping from 17 Hz at U_r = 6 to 27 Hz at U_r = 8.1. Between them is the transition zone where competition between two vibration frequencies is observed. Fig. 11 is a better presentation for such an observation. The competition and evolution at consecutive reduced velocities is evident here. Following this trend, the second jump and competition is discovered at a reduced velocity around 11. This is also the case and even more obvious when the mass ratio is increased to 3.4, as shown in the bottom left of Fig. 10. Jumps and competitions are observed at reduced velocity regions around 7 and 15, with a broader range around U_r = 15. This phenomenon was previously reported by Li *et al*. [33] in a study on a flexible cylinder with mass ratio of 4.3. They concluded the mode transition is accompanied with continuous change in amplitude, but also a jump in frequency. The overall distribution of case M-3.4 is significantly different from the cases with lower mass ratio. No amplitude peak is found at $U_r \approx 6$, but instead one is found at $U_r \approx 11$. One can also find that there are two main response frequencies involving in M-3.4's response in reduced velocity ranges of [5, 7] and [16, 25], which does not exist in case M-0.7 and M-1.0. Difference is also discovered in the increase rate of vibration frequency. Unlike cases M-0.7 and M-1.0, while increasing reduced velocity, the vibration frequency of case M-3.4 seems to stay steady, with a small increment outside competition regions. It is worth mentioning that with in-creasing reduced velocity, the maximum vibration frequencies for three cases are all found to be around 60 Hz. It seems the cylinder is limited from vibrating at a frequency beyond that value. A possible reason for this is that the cylinder switches from a tensioned-dominated cable at low reduced velocity (flow speed) to a bending-

dominated beam at high reduced velocity. As explained by Lee & Allen [24], the increased flow speed tends to induce larger de-flection on the structure. The resistance to this tendency comes primarily from the tension for a tension-dominated structure, or from the flexural stiffness, *EI*, for a bending-dominated one. As the tension is expected to rise due to increased flow velocity, the natural frequency, and thus the vibration frequency of a tension-dominated structure rises with flow speeds. However, this is not the case for flexural stiffness, *EI*, as it will not be affected by flow speed, which in turn means the flow speed has limited influence on the response frequency. Another significant difference is that when the mass ratio falls below 1, the amplitude peak is remarkable compared to other region. But with increasing mass ratio, this peak becomes considerably less notable.

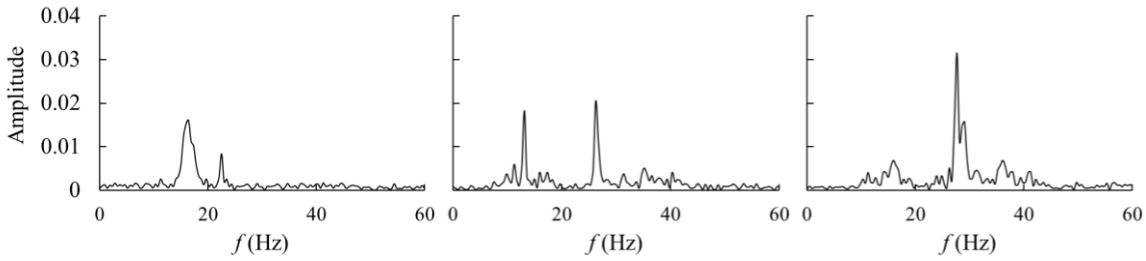

Fig. 11. Response spectra of case M-1.0 at U_r = 6.5, 7.5, and 8.1 from left to right.

As for the cross-flow response shown in the right column of Fig. 10, two amplitude peaks are found in case M-0.7 and 1.0 while three peaks in M-3.4 across the tested reduced velocity range, among which the first peaks of case M-0.7 and M-1.0 are found at $U_r \approx 5$, while M-3.4 found at around 7. In fact, the change in the spectra amplitude with respect to reduced velocity indicates the vibration mode transition. Take case M-3.4 as an example. It experiences two sets of high amplitude vibration in reduced velocity range of [4, 11] and [16, 25], between which exists vibration with low amplitude.

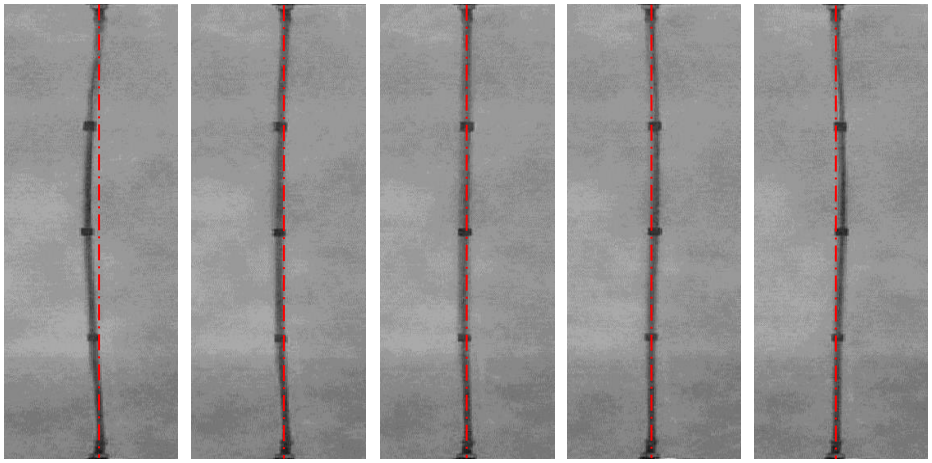

(*a*) 1st mode at U_r = 7.3.

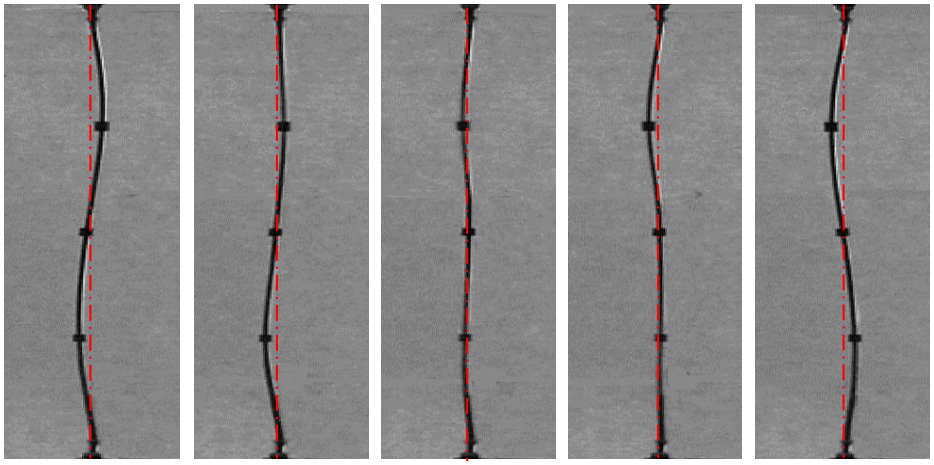

(*b*) 2nd mode at U_r = 13.8.

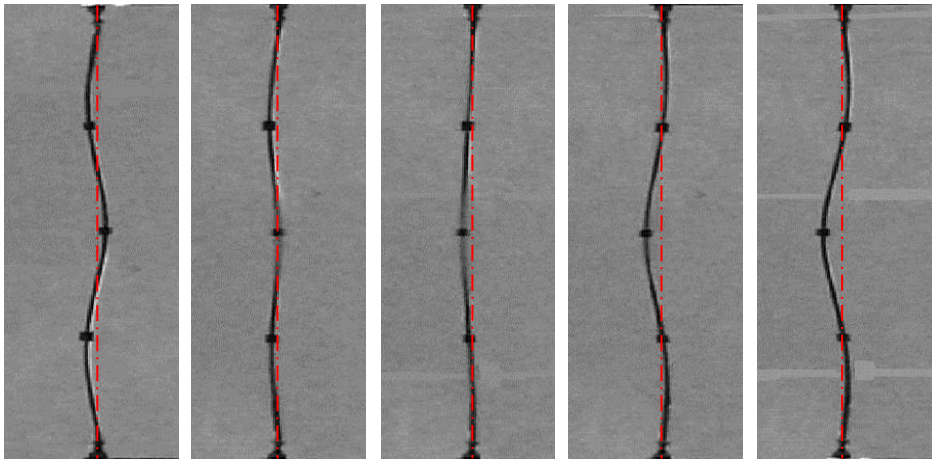

(*c*) 3rd mode at U_r = 17.7.

Fig. 12. Consecutive frames showing the cylinder (M-3.4) vibrating at different modes.

The first and second high amplitude range indicates the cylinder is vibrating at its 1st and 3rd structural modes respectively, while the low one indicates a 2nd mode, at which the mid-span (S-0.50) is a node in the structural mode and thus has low amplitude. This is confirmed by analyzing the obtained video. As demonstrated in Fig. 12, from top to bottom are consecutive frames taken from the recorded video at reduced velocity of 7.3, 13.8 and 17.7, clearly displaying the cylinder vibrating at its 1st, 2nd and 3rd mode respectively. It is clear that for every vibration mode, one can expect a peak in the spectra amplitude, though for locations at the node of the mode, the peak is considerably smaller than that of anti-nodes. From a general and qualitative point of view, the vibration mode has strong dependency on the Reynolds number: the higher Reynolds number, the higher the vibration mode it may reach. Up to the 3rd vibration mode is excited at the high Reynolds number under consideration. With respect to reduced velocity, the first mode transition (from the 1st to 2nd) takes place at $U_r \approx 15, 13, 11$ for case M-0.7, M-1.0, and M-3.4 respectively. There seems to be a trend that higher mass ratios lead to earlier mode transition with respect to reduced velocity. Similar to that of in-line response, the cross-flow response frequency also seems to be limited below 30 Hz for the three cases tested.

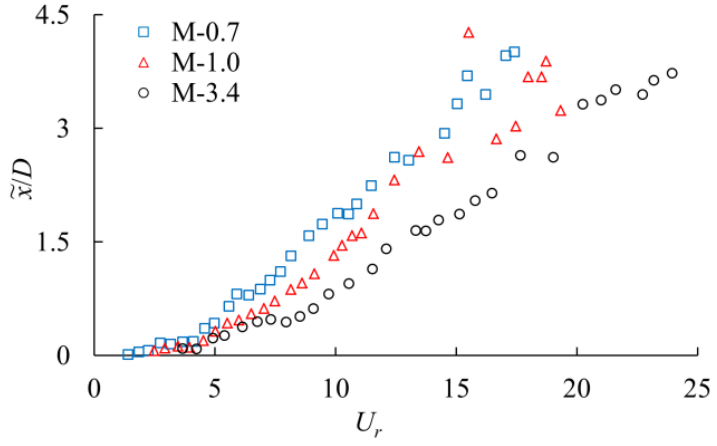

Fig. 13. Spatio-temporal RMS of normalized in-line displacements versus reduced velocity.

3.4 Vibration amplitudes & frequencies

Figure 13 presents the spatio-temporal root mean square (RMS) of the dimensionless in-line response displacement computed as

$$\tilde{x} = \sqrt{\frac{1}{S}\sum_{i=1}^{S}\left[\frac{1}{N}\sum_{j=1}^{N} u_{ji}^{2}(z,t)\right]} \tag{3.6}$$

Here, S is the number of samples in the selected time window for analysis and N is the number of measurement points along the axis of the cylinder, which is 3 in the present study. One can observe that the spatio-temporal RMS of the in-line vibration displacement has strong dependence on reduced velocity and generally follows quadratic trends for the three cases, with the lower mass ratio cases having considerably larger value. Similar trends were previously reported by Chaplin *et al*. [26] and Huera-Huarte & Bearman [27]. It is a result from the increased drag and tension, T, on the towed cylinder. Under increasing towing velocities, the cylinder experiences increasing drags and consequently higher tensions. It is known that the drag on the cylinder is balanced by the sum of horizontal components of tension, which is proportional to the product of $\tilde{x} \cdot T$. This yields

$$\tilde{x} \cdot T = C_1 \cdot C_d \cdot U^2 \tag{3.7}$$

where, C_1 is a constant coefficient; C_d is the drag coefficient. Considering the cylinder's modal frequencies are generally proportional to the square root of the tension, the below relationship is true upon the assumption of constant drag coefficient:

$$\tilde{x}/D = C_2 \cdot \left(\frac{U}{f_n \cdot D}\right)^2 \tag{3.8}$$

with C_2 a constant coefficient. This could help establish a rough estimation on the mean deflection of a flexible underwater cylinder on the design stage.

In the present work, to quantify the general vibration amplitude of the flexible cylinder, spatio-temporal standard deviations of displacement are computed to describe both the in-line and cross-flow responses. They are calculated as follows,

$$A_x = \sqrt{\frac{1}{S}\sum_{i=1}^{S}\left[\frac{1}{N}\sum_{j=1}^{N}[u_{ji}(z,t)-\overline{u_i}(z)]^2\right]} \tag{3.9}$$

$$A_y = \sqrt{\frac{1}{S}\sum_{i=1}^{S}\left[\frac{1}{N}\sum_{j=1}^{N}v_{ji}^2(z,t)\right]} \tag{3.10}$$

with A_x representing the in-line response amplitude; A_y for the cross-flow one.

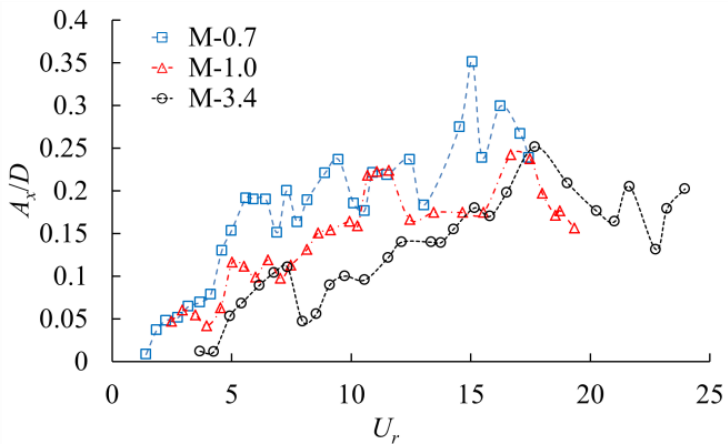

Fig. 14. Normalized in-line response amplitude versus reduced velocity.

The dimensionless spatio-temporal standard deviation of the in-line and cross-flow response expressed with respect to reduced velocity is shown in Figs. 14 & 15. High scatter is found existing in the data set. As the tested cylinder in the present work has low mass ratio, the added mass is expected to be comparable to its structural mass and thus have significant influence on the overall response by affecting the in-motion cylinder's

natural frequencies. Therefore, the high scatter in the response amplitude could be one of the consequences of the potential non-uniform distribution of the added mass and the resulting hydrodynamics.

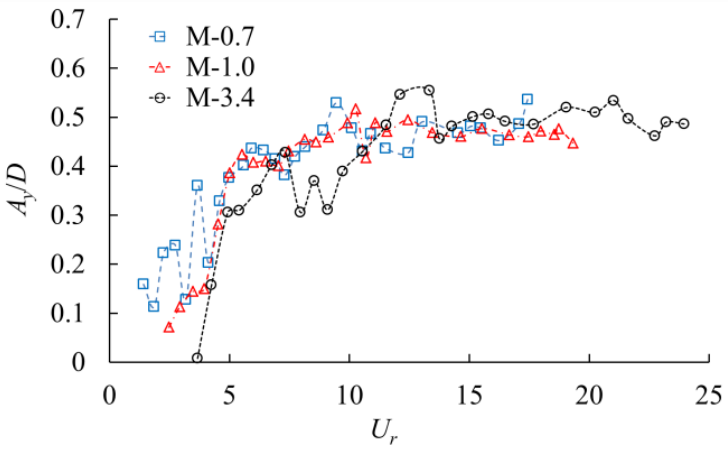

Fig. 15. Normalized cross-flow response amplitude versus reduced velocity.

As far as the in-line response amplitude is concerned, one of the evident effects of mass ratio on the cylinder's vibration is the generally increased response amplitude. It is clear that case M-0.7 is vibrating at an amplitude considerably larger than M-3.4. Case M-0.7 achieves maximum amplitude around 0.35*D*, while M-3.4 can only reach 0.25*D*. All three cases' response amplitudes start to rise as reduced velocity increases from 2, and reach their first peaks at $U_r \approx 6$. After this point, cases of M-0.7 and M-1.0 remain vibrating at high amplitude with a slight increase, but case M-3.4 seems to experience a de-synchronization characterized by a drop in amplitude at $U_r \approx 8$. There exist only initial and upper branches in the response amplitude; the lower branch disappears for all three cases, which could imply lock-in persists over the tested range. This is similar to the finding from elastically mounted rigid cylinders with mass ratios below 0.54 [14, 18]. In his pioneering work on flexible cylinders, Vandiver [25] addressed an explanation for the

widened lock-in band-width in low mass ratio cases: the added mass coefficient decreases sharply as the reduced velocity increases [34], which means the total mass and thus the natural frequency of the cylinder will rise considerably, since the structural mass is very low. The consequence of that is the resonant response frequency increases with flow speed and this leads to the persistence of the lock-in region.

Similar to that of in-line response amplitude, only initial and upper branches are found existing in cross-flow response amplitude with large amplitude persisting from a reduced velocity of 6 for three cases. It should be pointed out that the de-synchronization for case M-3.4 at $U_r \approx 8$ is also observed in cross-flow response, leading to a drop in vibration amplitude. It returns synchronized again right after that region. Other than that, varying mass ratio seems to have little effect on the cross-flow vibration. Vibration amplitudes more than 0.5D are observed for all three cases. This is lower than 0.7D as reported in a study on a flexible cylinder with mass ratio of 1.8 by Huera-Huarte and Bearman [27].

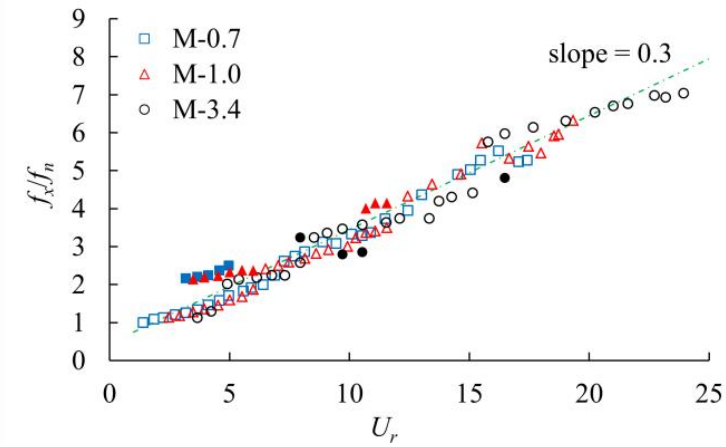

Fig. 16. Normalized in-line response frequency versus reduced velocity.

Dominant response frequencies that are the highest peaks in the spectra for every case were obtained by applying Fast Fourier Transform of the response displacement. The mean deflection in in-line response due to mean drag force was removed from the response displacement in advance. Figs. 16 & 17 presents the vibration frequencies of in-line and cross-flow response with respect to reduced velocity. In the plot of in-line response (Fig. 16), frequencies that have comparative magnitude to the dominant one are added as solid symbols as well.

One immediate observation from Figs. 16 & 17 is that the response frequencies rise linearly with reduced velocity, despite the variation in mass ratio. The slope for in-line and cross-flow responses is 0.3 and 0.15 respectively, which also indicates the frequency ratio between the in-line and cross-flow response is approximately 2.

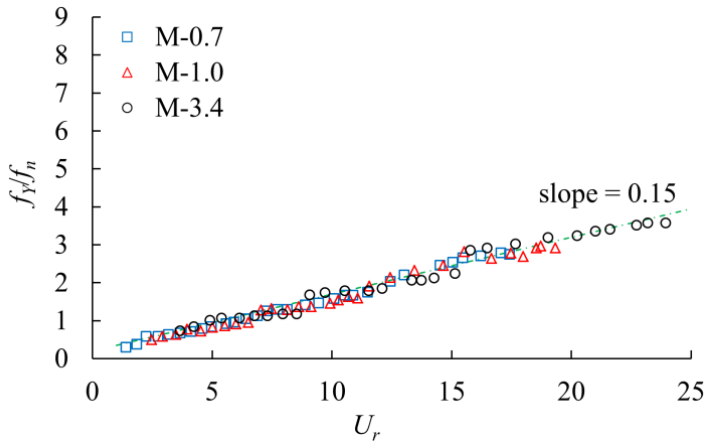

Fig. 17. Normalized cross-flow response frequency versus reduced velocity.

4 Conclusion

An experimental investigation of the effects of mass ratio on the hydrodynamic response of a highly flexible cylinder with 2 degrees of freedom undergoing cross flow-

induced vibration has been reported. Reynolds number range of 800 ~ 13,000, corresponding to reduced velocity range of 2 ~ 25 has been tested. Low values, namely 0.7, 1.0 and 3.4, of mass ratios were tested to investigate its effect. Multi-frequency vibration was discovered in the cylinder's dynamic response. The cylinder seemed to transition from tension-dominated at low reduced velocity to being bending dominated at high reduced velocity. Within the tested range, only the initial branch and upper branch were discovered in the response amplitudes of the in-line and cross-flow vibrations. After the initial rise, high amplitude responses were found to persist over the tested range because of the low value of mass ratio. An observed effect of mass ratio was the overall decreased amplitude in the in-line response. Limited influence was found on the cross-flow amplitude. Also examined was the vibration frequency. Linear relationships and independence of mass ratio was shown for normalized frequencies with respect to reduced velocities. Slope of 0.3 and 0.15 was revealed to predict the vibration frequency for in-line and cross-flow respectively. Correspondingly, the frequency ratio between in-line and cross-flow response was shown as approximately 2.

Acknowledgement

This work is made possible by Natural Sciences and Engineering Research Council of Canada.

References

[1] Blevins, R.D. (2001). Flow-induced vibration. Second ed. Krieger Publishing, Inc., Malabar, Florida, USA.

[2] Williamson, C.H.K., & Govardhan, R. (2004). Vortex-induced vibrations. *Annual Review of Fluid Mechanics*, **36**, 413–455.

[3] Williamson, C.H.K., & Govardhan, R. (2008). A brief review of recent results in vortex-induced vibrations. *Journal of Wind Engineering and Industrial Aerodynamics*, **96**(6), 713–735.

[4] Sarpkaya, T. (1979). Vortex-induced oscillations: a selective review. *Journal of Applied Mechanics*, **46**(2), 241–258.

[5] Sarpkaya, T. (2004). A critical review of the intrinsic nature of vortex-induced vibrations. *Journal of Fluids and Structures*, **19**(4), 389–447.

[6] Gabbai, R.D., & Benaroya, H. (2005). An overview of modeling and experiments of vortex-induced vibration of circular cylinders. *Journal of Sound and Vibration*, **282**(3), 575–616.

[7] Bearman, P.W. (1984). Vortex shedding from oscillating bluff bodies. *Annual Review of Fluid Mechanics*, **16**(1), 195–222.

[8] Bearman, P.W. (2011). Circular cylinder wakes and vortex-induced vibrations. *Journal of Fluids and Structures*, **27**(5), 648–658.

[9] Feng, C.C. (1968). The measurement of vortex induced effects in flow past stationary and oscillating circular and d-section cylinders. Master thesis, University of British Columbia, Vancouver, BC, Canada.

[10] Williamson, C.H.K., & Roshko, A. (1988). Vortex formation in the wake of an oscillating cylinder. *Journal of fluids and structures*, **2**(4), 355–381.

[11] Brika, D., & Laneville, A. (1993). Vortex-induced vibrations of a long flexible circular cylinder. *Journal of Fluid Mechanics*, **250**, 481–508.

[12] Govardhan, R., & Williamson, C.H.K. (2000). Modes of vortex formation and frequency response of a freely vibrating cylinder. *Journal of Fluid Mechanics*, **420**, 85–130.

[13] Khalak, A., & Williamson, C.H.K. (1996). Dynamics of a hydroelastic cylinder with very low mass and damping. *Journal of Fluids and Structures*, **10**(5), 455–472.

[14] Jauvtis, N., & Williamson, C.H.K. (2004). The effect of two degrees of freedom on vortex-induced vibration at low mass and damping. *Journal of Fluid Mechanics*, **509**, 23–62.

[15] Sumer, B.M., & Fredsoe, J. (1997). Hydrodynamics around cylindrical structures. World Scientific Publishing Co. Pte. Ltd., Singapore.

[16] Khalak, A., & Williamson, C.H.K. (1997). Fluid forces and dynamics of a hydroelastic structure with very low mass and damping. *Journal of Fluids and Structures*, **11**(8), 973–982.

[17] Khalak, A., & Williamson, C.H.K. (1999). Motions, forces and mode transitions in vortex-induced vibrations at low mass-damping. *Journal of Fluids and Structures*, **13**(7), 813–851.

[18] Jauvtis, N., & Williamson, C.H.K. (2003). Vortex-induced vibration of a cylinder with two degrees of freedom. *Journal of Fluids and Structures*, **17**(7), 1035–1042.

[19] Williamson, C.H.K. & Jauvtis, N., (2004). A high-amplitude 2T mode of vortex-induced vibration for a light body in XY motion. *European Journal of Mechanics B/Fluids*, **23**(1), 107–114.

[20] Vandiver, J.K. (1983). Drag coefficients of long flexible cylinders. In: *Offshore Technology Conference*. No. 4490-MS. Texas, USA.

[21] Kim, Y.H., Vandiver, J.K., & Holler, R. (1986). Vortex-induced vibration and drag coefficients of long cables subjected to sheared flows. *Journal of Energy Resources Technology*, **108**, 77–83.

[22] Chung, T.Y. (1987). Vortex-induced vibration of flexible cylinders in sheared flows. Ph.D. dissertation, Massachusetts Institute of Technology, Massachusetts, USA.

[23] Chung, T.Y. (1989). Vortex-induced vibration of flexible cylinders having different mass ratios. Report NO. UCE 440-1283ED, Korea Research Institute of Ships and Ocean Engineering.

[24] Lee, L., & Allen, D. (2010). Vibration frequency and lock-in bandwidth of tensioned, flexible cylinders experiencing vortex shedding. *Journal of Fluids and structures*, **26**(4), 602–610.

[25] Vandiver, J.K. (1993). Dimensionless parameters important to the prediction of vortex-induced vibration of long, flexible cylinders in ocean currents. *Journal of Fluids and Structures*, 7(5), 423–455.

[26] Chaplin, J.R., Bearman, P.W., Huarte, F.H., & Pattenden, R.J. (2005). Laboratory measurements of vortex-induced vibrations of a vertical tension riser in a stepped current. *Journal of Fluids and Structures*, **21**(1), 3–24.

[27] Huera-Huarte, F.J., & Bearman, P.W. (2009). Wake structures and vortex-induced vibrations of a long flexible cylinder–part 1: dynamic response. *Journal of Fluids and Structures*, **25**(6), 969–990.

[28] Chaplin, J.R., Bearman, P.W, Cheng, Y., Fontaine, E., Graham, J.M.R., Herfjord, K., Huera-Huarte, F.J., Isherwood, M., Lambrakos, K., Larsen, C.M., Meneghini, J.R., Moe, G., Pattenden, R.J., Triantafyllou, M.S., Willden, R.H.J. (2005). Blind predictions of laboratory measurements of vortex induced vibrations of a tension riser. *Journal of Fluids and Structures*, **21**(1), 25–40.

[29] Huera-Huarte, F.J., Bangash, Z.A., & Gonzalez, L.M. (2014). Towing tank experiments on the vortex-induced vibrations of low mass ratio long flexible cylinders. *Journal of Fluids and Structures*, **48**, 81–92.

[30] Farrant, T., Tan, M., & Price, W.G. (2001). A cell boundary element method applied to laminar vortex shedding from circular cylinders. *Computers & Fluids*, **30**(2), 211–236.

[31] Vandiver, J.K., Jaiswal, V., & Jhingran, V. (2009). Insights on vortex-induced, traveling waves on long risers. *Journal of Fluids and Structures*, **25**(4), 641–653.

[32] Song, J.N., Lu, L., Teng, B., Park, H.I., Tang, G.Q., & Wu, H. (2011). Laboratory tests of vortex-induced vibrations of a long flexible riser pipe subjected to uniform flow. *Ocean Engineering*, **38**(11), 1308–1322.

[33] Li, X., Wang, Y., Wang, G., Jiang, M., & Sun, Y. (2013). Mode transitions in vortex-induced vibrations of a flexible pipe near plane boundary. *Journal of Marine Science and Application*, **12**(3), 334–343.

[34] Sarpkaya, T. (1977). Transverse oscillations of a circular cylinder in uniform flow, Part I. Naval Postgraduate School Report, No. NPS-69SL77071.

CHAPTER IV

NUMERICAL SIMULATION OF FLOW-INDUCED VIBRATION ON A RIGID CYLINDER WITH TWO DEGREES OF FREEDOM

Haoyang Cen, Rupp Carriveau, and David S-K. Ting

Turbulence and Energy Laboratory, Ed Lumley Centre for Engineering Innovation, University of Windsor, Ontario, Canada

NOMENCLATURE

A_x	IL spatio-temporal response amplitude	m^*	Mass ratio
A_y	CF spatio-temporal response amplitude	Re	Reynolds number
CF	Cross-flow	U	Free stream velocity
D	Cylinder's outer diameter	U_r	Reduced velocity
f_x	IL vibration frequency	ζ_s	Damping ratio
f_y	CF vibration frequency	IL	In-line

1 Introduction

Fluid-structure interaction phenomena occur in many engineering fields, among which, flow-induced vibration is one of the fundamental problems. Particular research attention has been drawn to the case of circular cylinder mainly due to its extensive applications in engineering, such as power transmission lines, marine cables, mooring lines, and flexible risers in petroleum production. The current state and research effort in the field is well reviewed by Sarpkaya [1], Bearman [2], and also recent papers by Khalak & Williamson [3] and Govardhan & Williamson [4]. It is well known that an elastically mounted circular cylinder subject to oncoming flow exhibits several different types of responses, which is a joint result from a number of parameters. It includes the reduced velocity, Reynolds number, mass ratio, and damping ratio. Lock-in, in which case the vortex shedding frequency departs from the Strouhal frequency and follows the oscillation frequency, may occur in its vibration response and is one of the phenomenon that deserves great attention. This synchronization can lead to amplifications in cylinder's hydrodynamic response, and thus potentially destructive consequences.

A considerable amount of experimental studies has been carried out to investigate flow around a circular cylinder with two degrees of freedom (see e.g. [5-10]). However, these kinds of experiments are expensive to achieve, as it requires appropriate experimental facilities and instrumentations, which are usually at high prices. Therefore an attractive alternative is to utilize Computational Fluid Dynamics (CFD) as a tool to obtain the essential hydrodynamic quantities and flow structure information for engineering structure development. Anagnostopoulos [11] carried out a numerical simulation to investigate the hydrodynamic response and wake structure of a circular

cylinder undergoing flow-induced vibration in laminar flow. The Navier-Stokes equations were numerically solved via implementing a finite element scheme. The results obtained from his numerical simulation were revealed to be in a fairly good agreement with those obtained from experimental tests, except for those at reduced velocities above the lock-in region. Newman & Karniadakis [12, 13] performed direct numerical simulation (DNS) studies on flow past a freely vibrating cable. The implemented a body fitted coordinates for their solution and tested the cable at Reynolds numbers of 100 and 200. Guilmineau & Queutey [14] investigated FIV on a rigid circular cylinder with low mass-damping. The flow condition was turbulent and the SST κ-ω model was utilized to describe the flow. They considered three sets of scenario: (a) flow starting from rest; (b) increasing velocity; and (c) decreasing velocity. The lower branch was the only response amplitude branch predicted in the first and third sets tested scenario. Other than that, as the flow velocity rose, the cylinder progressively reaches its maximum vibration amplitude, which agreed to those reported from experimental studies. But discrepancies from experiment results were found in the response upper branch.

Placzek *et al*. [15] studied a circular cylinder with forced and freely vibration in flow with low Reynolds number. They analyzed the vortex shedding modes and established a relation with frequency response. Bahmani & Akbari [16] numerically investigated the hydrodynamic response characteristics and vortex shedding mode of a freely vibrating circular cylinder with two degrees of freedom in laminar flow. Bao *et al*. [17] presented interesting results of freely vibrating cylinders in isolated and tandem configurations. The cylinders were modeled with two degrees of freedom at a series of natural frequency ratios (in-line to cross-flow). Schulz & Meling [18] reported an

analysis on the fluid-structure interaction between a long flexible rise and turbulent flow. The problem was tackled using a multi-strip method, which was achieved by solving the two-dimensional Unsteady Reynolds-Averaged Navier-Stokes (URANS) equations concurrently with a finite element structural dynamic response model. The full three-dimensional structural analysis was realized by combining a couple of individual two-dimensional simulations on various section location along the riser. Overall hydrodynamic response in terms of resulted loads and displacement were predicted.

To date, not many numerical simulations have been performed to investigate the wake pattern around a circular cylinder with low mass ratio. More research effort is needed in the field.

2 Description of the problem

2.1 Computational domain and boundary conditions

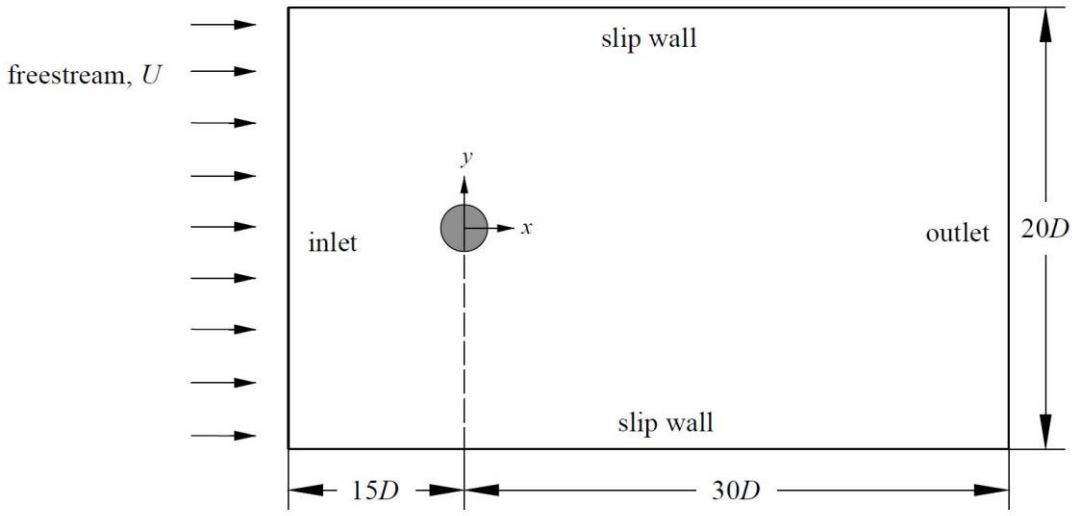

Fig. 1. Geometrical model and computational domain.

As depicted in Fig. 1, a circular cylinder standing in a rectangular flow field is under consideration in the present study. The distances from the inlet and outlet to the cylinder center are 15*D* and 30*D* respectively, with *D* being the diameter of the circular cylinder, while the lateral dimension of the fluid domain is 20*D*.

The boundary conditions employed for the present investigation are specified below. The inlet is specified with various constant stream-wise velocities, while the outlet is maintained with velocity gradients $\partial u/\partial x$ and $\partial v/\partial x$ being zero. In the present study, the cylinder diameter D = 8 mm; mass ratio m^* = 1.0; damping ratio ζ = 0.04; natural frequency $f_x = f_y$ = 5 Hz, and the Re number is from 530 to 3,200. Cylinder wall is specified to be impermeable with no-slip condition for flow velocity. The two side boundaries of the fluid domain are imposed with free-slip conditions. The Neumann condition is applied to the inlet and surface of the cylinder for pressure setting, while the outlet boundary is also imposed with pressure Dirichlet boundary.

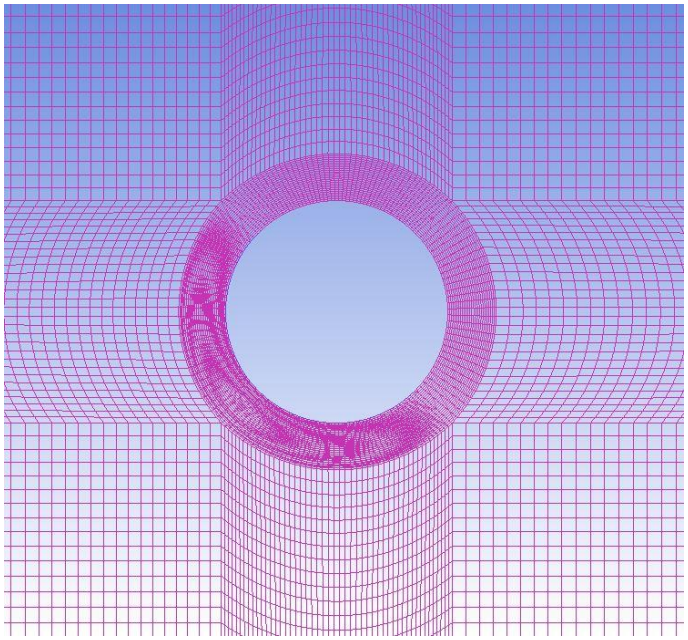

Fig.2. Generated mesh around the circular cylinder.

2.2 Generated mesh

For the achievement of accurate solution in a reasonable computation time, it is essential to establish a mesh with adequate flow resolution while maintaining computable number of mesh nodes. As such, relatively fine mesh is adopted in the downstream behind the cylinder as well as regions around it. Outside these regions, the mesh is constructed to be relatively coarse with lower resolution. This could help in dealing with any unexpected large mesh deformation. Bias is set towards to the wall of the cylinder, i.e., the mesh is placed denser near the wall of the cylinder, but it becomes gradually sparser as the distance between the wall and cell centre increases. It is critical to ensure the first layer grid thickness satisfies the condition that $y^+ = \frac{y}{\mu}\sqrt{\rho\tau_w} \approx 1$, where, y is the distance from the wall to the cell centre; u is the molecular viscosity, ρ is the density of the water; and τ_w is the wall shear stress. Based on that, the first grid size near the cylinder wall is determined to be $0.01D$, and the time step is set at 0.005 according to the courant-Friedrichs-Lewy (CFL) condition. Finally the generated mesh consists of 41000 nodes and 20000 elements. Fig. 2 presents the enlarged view of the mesh generated around the circular cylinder under consideration.

2.3 FSI solution of ANSYS

In the present study, the flow-induced vibration of a circular cylinder is simulated using Ansys Workbench. This platform couples the Fluent and Ansys Transient Structure to solve fluid-structure interaction model. It is equipped with a well-designed FSI solution scheme that is able to carry out tight integrations between the hydrodynamics

and structural response. It is a flexible and advanced tool for this kind of coupling problems. The solution scheme of the problem under consideration is presented in Fig. 3, showing the modules utilized in the present study as well as the connections between each of them. The Geometry module is set up for the construction of geometric models of both the cylinder and fluid domain. The information from the Geometry module is shared by the Transient Structural and Fluid Flow modules, where the structural response and hydrodynamics is solved respectively. For this analysis, FLUENT is utilized as the fluid solver. Upon the successful executions of the Transient Structure and Fluid Flow, the System Coupling module will start the coupled simulations. It performs as a coupling master process. Both the Transient Structure and Fluid Flow modules are connected to it for data communication. Once the communication is through, System Coupling transfer the data sequentially between Transient Structure and Fluid Flow at pre-defined synchronization points (SP), i.e., at each of this point, information of fluid dynamic loads is transferred to the Transient Structure via System Coupling; Transient Structure determines the cylinder's response based on the obtained fluid information and send the response information back to Fluid Flow thereafter. Upon the reception of the structural deformation data, the mesh in fluid domain will be updated (diffusion-based smoothing method is used in the present study). After convergence is reached, the coupled simulation proceeds to the next time step until the pre-set end time. The implicit coupling iteration is adopted to secure the consistency between the fluid and structure solution at the end of every coupling step, as such resulting in higher numerical solution stability [19]. Second Order Backward Euler scheme, which is an implicit time-stepping scheme,

is applied in the transient analysis as generally recommended for transient analysis in ANSYS FLUENT.

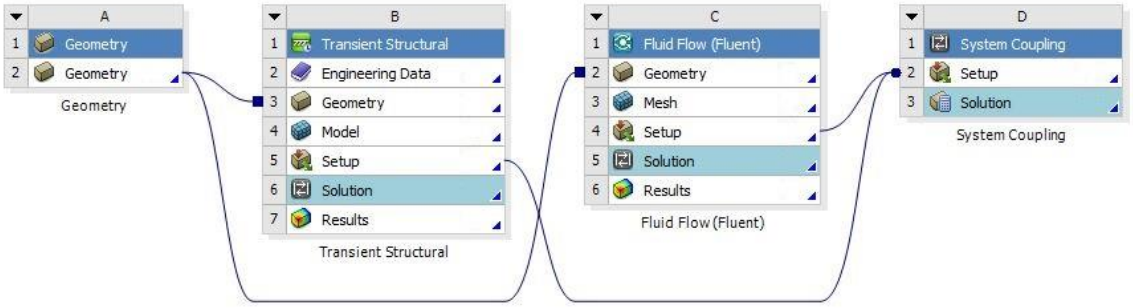

Fig. 3. Solution scheme in ANSYS WORKBENCH

3 Results and discussions

The FIV of an elastically mounted rigid cylinder is nonlinear. The fluid force generated by the vortex around the cylinder makes the cylinder vibrated; in turn, the oscillating cylinder also affects the flow field around it, eventually flow field changes the induced forces on the cylinder and hence the cylinder response. Normally the cylinder's response follows sinusoid wave trend at low reduced velocities, e.g., the time history of dimensionless cross-flow vibration amplitude shown in Fig. 4. But in some cases, instability indicated by beat phenomenon occurs in the cylinder's dynamic response. Fig. 5(a) presents the time history of the lift coefficient at U_r = 6.0, where distinct beat phenomenon is shown. Fast Fourier Transform is applied on this signal and the result is shown in Fig 5(b). Two distinct frequencies are dominating the cylinder's response, with one at approximately 18 Hz and the other at 23 Hz.

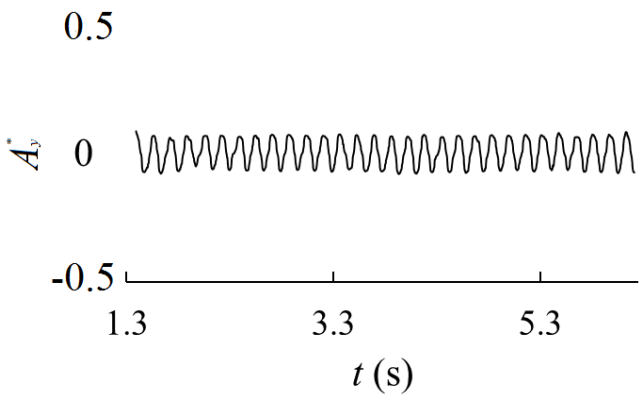

Fig. 4. Time history of dimensionless cross-flow response amplitude at U_r = 2.6.

Figs. 6 & 7 present the maximum vibration amplitude of the tested cylinder. It is clear that there exist initial, upper, and lower branch in both the in-line and cross-flow response. For both of them, the amplitude peaks at $U_r \approx 6.2$, with a value approaching to 0.36 for in-line response while 1.26 for cross-flow one. Right after this reduced velocity point, the cylinder experiences sharp reduction in its maximum vibration response. The in-line response drops to approximately 0.1, while the cross-flow one decreases to about 0.6. This is believed to due to the occurrence of lock-in by when considered concurrently with Fig. 8 that presents the normalized cross-flow response frequency. For a circular cylinder, it is well recognized that the vortex shedding frequency follows Strouhal frequency (f_{st}) when lock-in is not present. As the Strouhal frequency is calculated as

$$f_{st} = St \cdot (U / D), \tag{4.1}$$

One can expect the vortex shedding frequency will rise linearly with respect to flow velocity. This is evident in Fig. 8, where the normalized cross-flow response frequency rises linearly within the reduced velocity range of 2 to 7, but outside this range the response frequency starts to depart from Strouhal frequency with an almost constant value around 1.2.

(*a*)

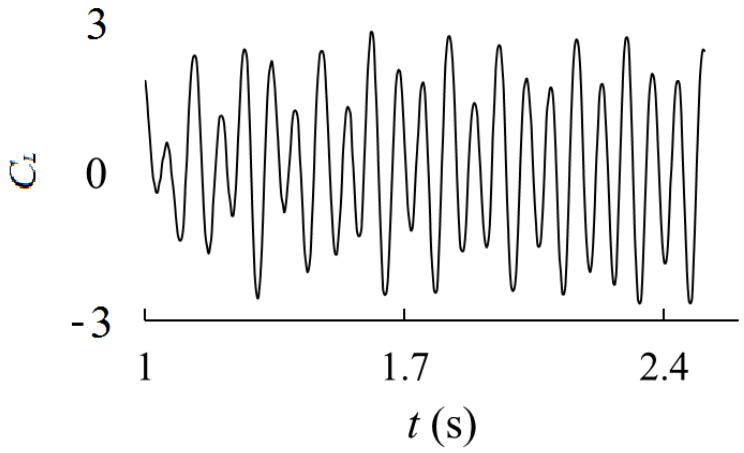

(*b*)

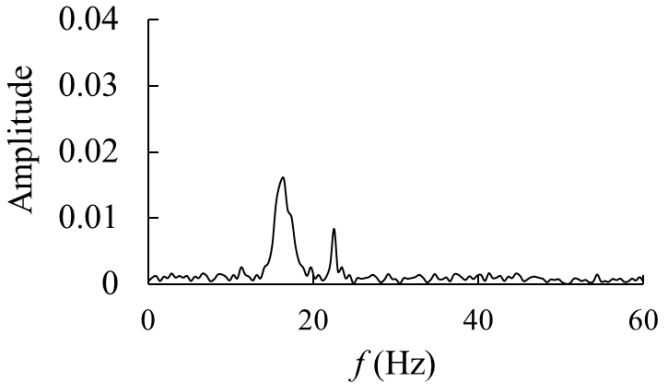

Fig. 5. Time history of lift coefficient at U_r = 6.0 and corresponding frequency spectrum.

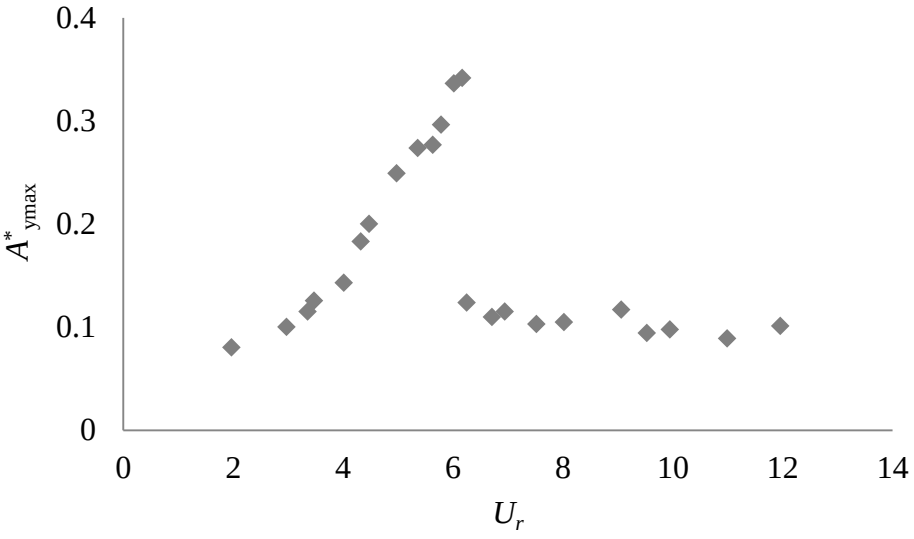

Fig. 6. Dimensionless in-line response amplitude versus reduced velocity.

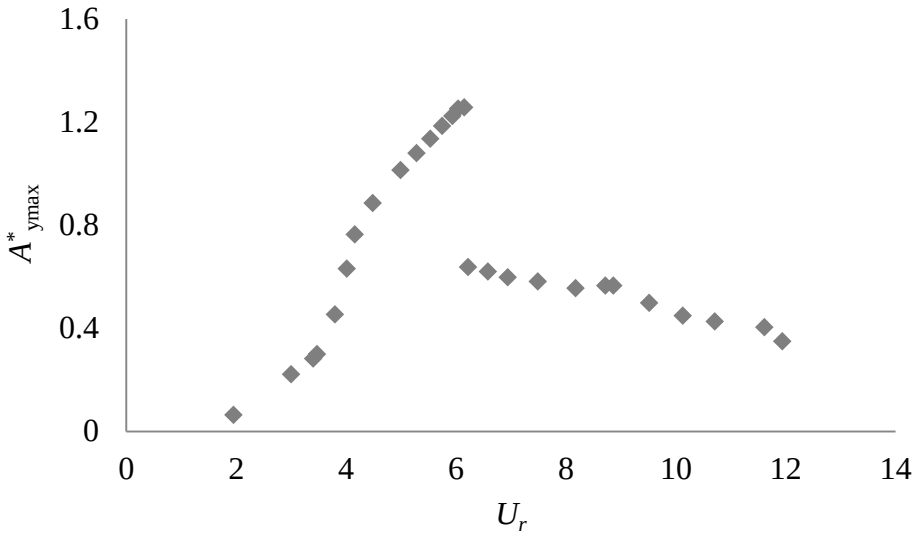

Fig. 7. Dimensionless cross-flow response amplitude versus reduced velocity.

Figure 9 shows the periodical trajectory of the elastic cylinder at different Reynolds number. These plots clearly show that the oscillations are self-limiting and they all appear to have a "Figure 8" shape except for the one at Re = 1800.

In Fig. 10, the downstream wake structures are presented. At low reduced velocity, the cylinder is starting to vibrate. Both in-line and cross-flow vibration are not influential at this moment, with a very low amplitude. With the flow velocity increasing to U_r = 4.8, the Karman vortex street is formed behind the cylinder, and it causes uneven pressure distribution at two sides, leading to an excited cylinder. In this case, the wake transition to a 2S mode (see Fig. 10(*a*)), with one single vortices shedding from each side of the cylinder every half cycle. When the reduced velocity keep increasing to around 6, where the cylinder exhibit maximum response amplitude, the vortex shedding turn into a 2T mode, with 2 sets of triple shedding from the cylinder every cycle. 2P vortex shedding mode, where 2 pairs of vortices flow to downstream every cycle, is found existing at U_r higher than 6.

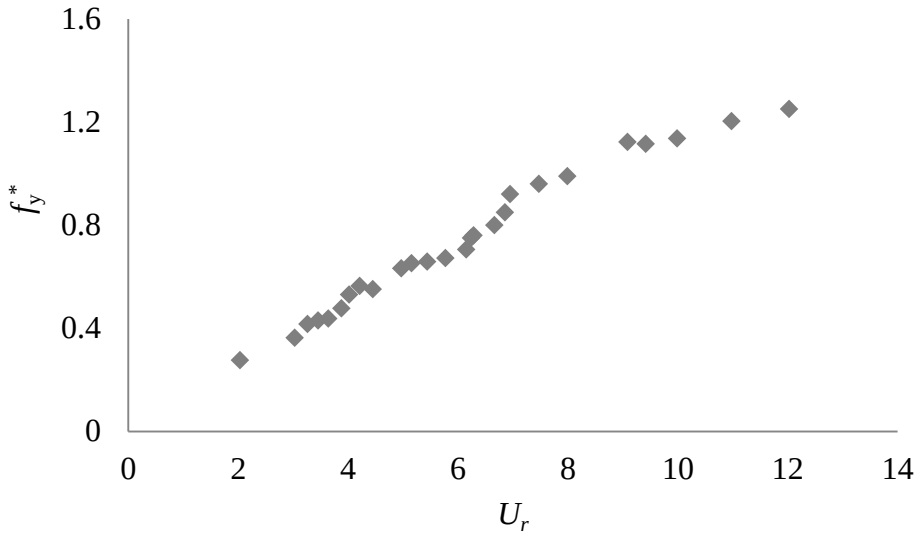

Fig. 8. Normalized cross-flow response amplitude versus reduced velocity.

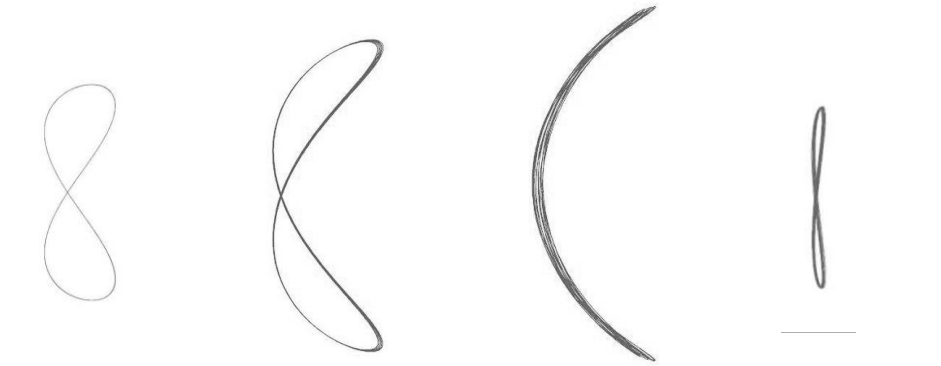

Fig. 9. Cylinder's vibration trajectory at different Reynolds number.

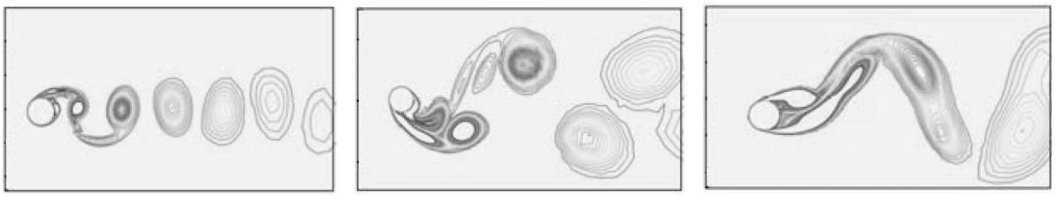

Fig. 10. Downstream flow structure.

4 Conclusion

A numerical simulation has been carried out on the fluid-structure interaction of an immerged smooth circular cylinder with two degrees of freedom at Reynolds number ranging from 530 to 3200 using the SST $\kappa-\omega$ turbulent model. With the mass ratio being 1, the cylinder has a natural frequency ratio (in-line/cross-flow) of 1. Initial, upper, and lower branches are found in the cylinder's response amplitude for both the in-line and cross-flow directions. At most of the tested velocities, the cylinder exhibits a "Figure 8" trajectory, except for those velocities where the cylinder had large response amplitudes. The present study also presents the flow structure downstream the cylinder, demonstrating "SS", "2S", "2T", and "2P" vortex shedding modes.

References

[1] Sarpkaya, T. (2004). A critical review of the intrinsic nature of vortex-induced vibrations. *Journal of Fluids and Structures*, **19**(4), 389–447.

[2] Bearman, P.W. (1984). Vortex shedding from oscillating bluff bodies. *Annual Review of Fluid Mechanics*, **16**(1), 195–222.

[3] Khalak, A., & Williamson, C.H.K. (1999). Motions, forces and mode transitions in vortex-induced vibrations at low mass-damping. *Journal of Fluids and Structures*, **13**(7), 813–851.

[4] Govardhan, R., & Williamson, C.H.K. (2000). Modes of vortex formation and frequency response of a freely vibrating cylinder. *Journal of Fluid Mechanics*, **420**, 85–130.

[5] Bearman, P.W. (2011). Circular cylinder wakes and vortex-induced vibrations. *Journal of Fluids and Structures*, **27**(5), 648–658.

[6] Williamson, C.H.K., & Roshko, A. (1988). Vortex formation in the wake of an oscillating cylinder. *Journal of Fluids and Structures*, **2**(4), 355–381.

[7] Govardhan, R., & Williamson, C.H.K. (2000). Modes of vortex formation and frequency response of a freely vibrating cylinder. *Journal of Fluid Mechanics*, **420**, 85–130.

[8] Dahl, J.M., Hover, F.S., & Triantafyllou, M.S. (2006). Two-degree-of-freedom vortex-induced vibrations using a force assisted apparatus. *Journal of Fluids and Structures*, **22**(6), 807–818.

[9] Jauvtis, N., & Williamson, C.H.K. (2004). The effect of two degrees of freedom on vortex-induced vibration at low mass and damping. *Journal of Fluid Mechanics*, **509**, 23–62.

[10] Khalak, A., & Williamson, C.H.K. (1997). Fluid forces and dynamics of a hydroelastic structure with very low mass and damping. *Journal of Fluids and Structures*, **11**(8), 973–982.

[11] Anagnostopoulos, P. (1994). Numerical investigation of response and wake characteristics of a vortex-excited cylinder in a uniform stream. *Journal of Fluids and Structures*, **8**(4), 367–390.

[12] Newman, D., & Karniadakis, G.E. (1996). Simulations of flow over a flexible cable: a comparison of forced and flow-induced vibration. *Journal of Fluids and Structures*, **10**(5), 439–453.

[13] Newman, D.J., & Karniadakis, G.E. (1997). A direct numerical simulation study of flow past a freely vibrating cable. *Journal of Fluid Mechanics*, **344**, 95–136.

[14] Guilmineau, E., & Queutey, P. (2004). Numerical simulation of vortex-induced vibration of a circular cylinder with low mass-damping in a turbulent flow. *Journal of Fluids and Structures*, **19**(4), 449–466.

[15] Placzek, A., Sigrist, J.F., & Hamdouni, A. (2009). Numerical simulation of an oscillating cylinder in a cross-flow at low Reynolds number: Forced and free oscillations. *Computers & Fluids*, **38**(1), 80–100.

[16] Bahmani, M.H., & Akbari, M.H. (2010). Effects of mass and damping ratios on VIV of a circular cylinder. *Ocean Engineering*, **37**(5), 511–519.

[17] Bao, Y., Huang, C., Zhou, D., Tu, J., & Han, Z. (2012). Two-degree-of-freedom flow-induced vibrations on isolated and tandem cylinders with varying natural frequency ratios. *Journal of Fluids and Structures*, **35**, 50–75.

[18] Schulz, K.W., & Meling, T.S. (2004). Multi-strip numerical analysis for flexible riser response. In: Proceedings of the 23rd international conference on offshore mechanics and arctic engineering. OMAE2004-51186, Vancouver, Canada.

[19] ANSYS. ANSYS system coupling guide; 2013.

CHAPTER V

CONCLUSIONS AND RECOMMEDNED FUTURE WORK

1 Conclusions

With the increasingly extensive offshore exploration, it is critical to enhance our understanding in the interaction mechanism of flow-induced vibration on flexible cylinder and to ensure offshore flexible cylindrical structures to be well designed in terms of performance, reliability, and costs. To achieve that, studies on the influential parameters (axial pre-tension and mass ratio) of the phenomenon have been carried out and presented in this thesis.

Experimental investigations have been conducted on a flexible circular cylinder with two degrees of freedom undergoing cross flow-induced vibration using optical measurement technique. In Chapter II, the effect of axial pre-tension has been tested by imposing three different axial pre-tensions, namely 0, 4 and 8 N on the cylinder separately. The flexible cylinder with mass ratio of 0.77 has been tested at Reynolds number from 780 to 6300, corresponding to reduced velocity range of 2 to 16. The vibration amplitudes and frequencies have been quantified. The results reveal that higher pre-tension is able to decrease the vibration amplitudes, in particular the cross flow one. The lock-in bandwidth in the in-line response is narrowed when the pre-tension is high. Though the vibration frequencies is found to rise with increasing pre-tension,

independence of pre-tension is demonstrated in frequency ratios, which rises linearly with respect to reduced velocity. The slopes of linear fitting are 0.28 and 0.14 for IL and CF motions respectively. The ratio of IL response frequency to CF one remained at approximately 2 within the tested range despite the changes in pre-tension.

In Chapter III, the effects of mass ratio has been studied and reported. The flexible cylinder has been tested at Reynolds number range of 800 ~ 13,000, corresponding to reduced velocity range of 2 ~ 25. Realistic mass ratios, namely 0.7, 1.0, and 3.4 have been studied. Within the tested range, only the initial and upper branches appear in the response amplitudes of both the in-line and cross-flow vibrations. High amplitude responses persist over the tested range after the initial rise. Low value mass ratio is revealed to be able to decrease the amplitude in the in-line response but rather limited in the cross-flow one. Similar to that in Chapter II, linear relationships and independence of mass ratio are found in the normalized frequencies with respect to reduced velocity. However, the slopes found in this set of experiment are 0.3 and 0.15 for the in-line and cross-flow response respectively.

Numerical simulation has also been attempted to investigate the wake patterns behind a circular cylinder in a 2-dimensional scenario. To explore the possibility of study this phenomenon numerically, the numerical model in the present work has been built to represent the experimental model. The results present four distinct vortex shedding modes behind a rigid circular cylinder, namely, “SS”, “2S”, “2T”, and “2P”.

2 Recommended future work

The findings of the present work mainly serve as addition to the knowledge of flow-induced vibration on a flexible circular cylinder. Since applications of flexible cylinders in offshore engineering are expanding at a high speed in recent decades, the information revealed from the present thesis enhances our knowledge in the field. This is essential and critical in offshore structures development and can help solidify the future of offshore industry. While the experiments conducted presented the general vibration characteristics of a flexible cylinder undergoing flow-induced vibration in uniform flow and the numerical simulation demonstrated the wake pattern in a 2-dimensional scenario, the below future work is recommended to enhance our understanding in the field.

2.1 Sheared flow

Most of offshore structures encounter sheared flows at their practical services. It is well known that sheared flow is able to induce more complex vibration on flexible cylinder. In addition to providing more insights in realistic scenario, experiment of flexible cylinder under sheared flow condition is necessary to generate quality data for the validation of numerical and empirical studies. The current experimental setup is encouraged to extend to sheared flow conditions. Concurrently with the information presented in this thesis, this would improve our understanding of the underlying mechanism.

2.2 Downstream flow structure

As the uneven pressure distribution associated with the wake behind a flexible cylinder is one of the major contributors to the flow-induced vibration, it would be beneficial and interesting to investigate the flow structure behind a flexible cylinder. In the Chapter III of this thesis, the high amplitude vibration was suspected to be caused by lock-in. But without the knowledge of vortex shedding frequency in the wake, no one can be sure about that. By illuminating the downstream flow structure, it will deliver the necessary knowledge of vortex shedding frequency to certify the occurrence of lock-in.

2.3 Three-dimensional simulation

While 2-dimensional simulation has been carried out in this thesis, the model should be extended to a 3-dimensional scenario to fully capture the flow structure and cylinder modal characteristics. Computational Fluid Dynamics is a powerful and promising tool for the analysis of flow-induced vibration, as it could possibly reduce the times of conducting experimental work, which for offshore structure research would normally require expensive facilities and instrumentations. The main issue for now is that computation time required for such a problem is overwhelming for academic research, not to mention the industry that is chasing for effectiveness and efficiency. Therefore, it is meaningful to develop high-performance computer and high-efficiency solution algorithm to make the three-dimensional simulation realistic in both academic researches and industrial projects.

APPENDIX A

DETERMINATION OF TOWING SPEED

The following content describes the determination of the towing speed in the experiments presented in this thesis.

Prior to experiments, the towing tank utilized is marked with fluorescent tapes on the bottom to identify the instantaneous location of the cylinder. As illustrated in Fig. 1, the fluorescent tapes are placed on one side of the tank floor and aligned along its length at a distance of 25 mm.

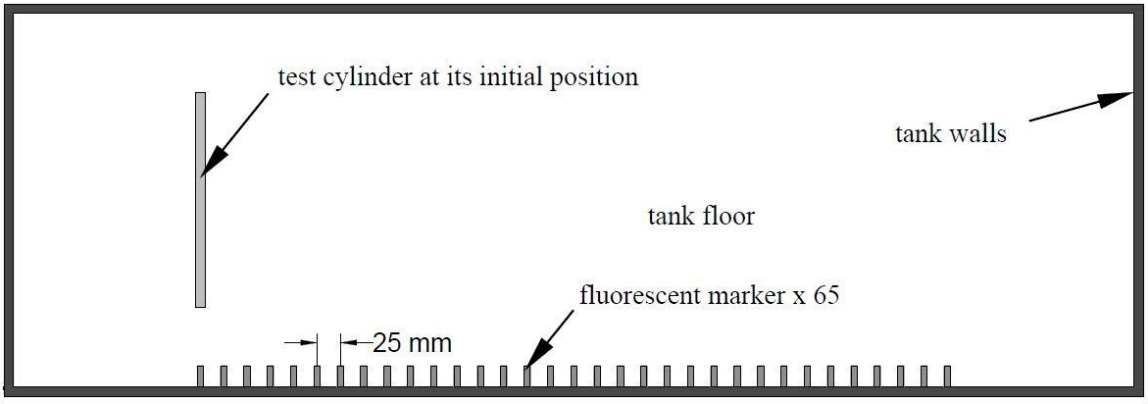

Fig. 1. Illustration of fluorescent marker for speed determination.

As such, to determine the towing speed U_{t1} at the time t_1, we only need to identify the n^{th} fluorescent marker at that moment and the m^{th} marker at the next time instance, t_2. Then the towing speed is calculated as

$$U_{t1} = \frac{(m-n)\times 25}{t_2 - t_1} mm/s \tag{A.1}$$

VITA AUCTORIS

NAME:	Haoyang Cen
PLACE OF BIRTH:	China
YEAR OF BIRTH:	1989
EDUCATION:	South China University of Technology, B.Eng., Guangzhou, China, 2013
	University of Windsor, M.A.Sc., Windsor, ON, 2015